의학석사 학위논문

A Hepatitis B Virus-derived Peptide Exerts an Anticancer Effect via TNF/iNOS-producing Dendritic Cells in Tumor-bearing Mouse Model

B형 간염 바이러스 중합효소 유래 펩타이드의 TNF 및 iNOS 발현 수지상세포 활성화를 통한 항암 효과에 관한 연구

2021년 2월

서울대학교 대학원

의과학과 의과학전공

양 수 빈

B형 간염 바이러스 중합효소 유래 펩타이드의 TNF 및 iNOS 발현 수지상세포 활성화를 통한 항암 효과에 관한 연구

지도교수 김 범 준

이 논문을 의학석사 학위논문으로 제출함
2021년 1월

서울대학교 대학원
의과학과 의과학전공
양 수 빈

양수빈의 의학석사 학위논문을 인준함
2021년 1월

위 원 장 국 윤 호 (인)

부위원장 김 범 준 (인)

위 원 한 응 수 (인)

A Hepatitis B Virus-derived Peptide Exerts an Anticancer Effect via TNF/iNOS-producing Dendritic Cells in Tumor-bearing Mouse Model

by

Soo-Bin Yang

A thesis submitted to the Department of Medicine
in partial fulfillment of the requirements for the
Degree of Master of Science in Medicine
at Seoul National University

January, 2021

Confirming the Master's thesis written by
Soo-Bin Yang
January, 2021

Approved by Thesis committee :

Professor _____ (Seal)
Professor _____ (Seal)
Professor _____ (Seal)

ABSTRACT

Recently, a 6-mer hepatitis B virus (HBV)-derived peptide, Poly6 has been reported to exert antiviral effects against human immunodeficiency virus type 1 (HIV-1). Here, the immuno-therapeutic potential of Poly6 was explored via its administration into dendritic cells (DCs) in a mouse model. Data revealed that Poly6 treatment led to enhanced production of tumor necrosis factor (TNF) and inducible nitric oxide synthase (iNOS)-producing DCs (Tip-DCs) in a type 1 interferon (IFN-I)-dependent manner via the induction of mitochondrial stress. Poly6 treatment in mice implanted with MC38 cells, a murine colon adenocarcinoma line, led to attenuated tumor formation, primarily due to direct cell death induced by Tip-DC mediated nitric oxide (NO) production and indirect killing by Tip-DC mediated cluster of differentiation 8 (CD8) cytotoxic T lymphocyte (CTL) activation via CD40 activation. Moreover, Poly6 treatment demonstrated an enhanced anticancer effect with one of the checkpoint inhibitors, the anti PD-L1 antibody. In conclusion, Poly6 single treatment represents the anticancer effects through Tip-DC activation, that suggest a potential as an anti-cancer peptide. Also, Poly6 represents a

potential adjuvant for cancer immunotherapy by enhancing the anticancer effects of immune checkpoint inhibitors.

Keywords: HBV-derived Poly6 peptide, TNF/iNOS-producing DC (Tip-DC), Type 1 interferon (IFN-I), CD40, Cancer immunotherapy

Student Number: 2018-23838

CONTENTS

LIST OF TABLES AND FIGURES

LIST OF ABBREVIATIONS

8-OHdG : hydroxyl-2' -deoxyguanosine

Ab :Antibody

ACT : adoptive cell transfer

Ag : antigen

APC : antigen presenting cell

Arg1 : Arginase 1

BMDC : bone marrow derived dendritic cell

cGAS : cyclic GMP-AMP synthase

CFSE : carboxyfluorescein succinimidyl ester

CTL : cytotoxic T lymphocyte

DC : Dendritic cell

ELISA : enzyme-linked immunosorbent assay

HAT : histone acetylation transferases

HBV : Hepatitis B Virus

HDAC : histone deacetylases

HIV : human immunodeficiency virus

H&E : hematoxylin and eosin staining assay

IFN-I : Type 1 Interferon

iNOS : inducible nitric oxide synthase

IRF-3 : Interferon regulatory factor 3

IV : intravenous

KO : Knock out

L-NAME : N omega-Nitro-L-arginine methyl ester hydrochloride

LPS : Lipopolysaccharides

MDSC : myeloid derived suppressor cell

mt ROS : mitochondrial reactive oxygen species

NO : nitric oxide

NOS2 : nitric oxide synthase 2

qRT-PCR : quantitative real-time polymerase chain reaction

SC : subcutaneous

STAT-1 : Signal transducer and activator of transcription 1

STING : stimulator of interferon genes

TAM : tumor associated macrophage

Th cell : effector T helper cell

Tip-DC : TNF- α and iNOS -producing DC

TNF- α : Tumor necrosis factor- α

TUNEL : terminal deoxynucleotidyl transferase-mediated dUTP nick-end labeling

W4P-LHB-NIH3T3 cell : HBV W4P large surface protein -expressing NIH-3T3 cell

INTRODUCTION

Since it has fewer side effects than those of other cancer therapies and can be administered for various cancers, immunotherapy is a promising replacement of other treatments or an adjunctive therapy that enhances the treatment efficacy of other cancer therapies [1, 2]. However, the ability of tumors to escape the immune system due to the immunosuppressive tumor microenvironment remains a major obstacle in cancer immunotherapy [3]. Local immunosuppression of T cells is a major part of antitumor potential in the tumor microenvironment and is elicited by cells from the mononuclear phagocytic system, such as myeloid derived suppressor cells (MDSCs) and tumor-associated macrophages (TAMs) [4-6]. Therefore, introducing tools that can reverse the immunosuppressive phenotype is central to harnessing the power of immunotherapeutic strategies.

Dendritic cells (DCs) are potent antigen presenting cells (APCs) that play a pivotal role in antitumor immune responses [7]. Following the capture of antigens, mature DCs exert strong antitumor effects by inducing cancer specific adaptive immune response through the release of IL-12 or by cross-presentation of exogenous cancer antigens on MHC class Ⅰ molecules [8]. For the

effective cancer treatment, immunotherapy is aimed at inducing cancer Ag-specific immune responses that can induce the death of cancer cells [9]. To achieve this, it is critical to reprogram APCs, particularly DCs, to recover immune tolerance of cytotoxic T lymphocytes (CTL) and effector T helper (Th) cells specific to cancer Ags in the tumor microenvironment [10, 11].

Tumor-associated myeloid cells inhibit antitumor T cell responses in the tumor microenvironment primarily by inhibitory pathways involving the metabolism of arginine through the regulated expression of two enzymes: arginase 1 (ARG1, encoded by ARG1), which hydrolyzes arginine, and nitric oxide synthase 2 (NOS2, also known as inducible NOS or iNOS), which generates nitric oxide (NO) from arginine and oxygen [12]. Even though the precise roles of NOS2 and its reaction products in promoting or controlling cancer are still controversial, a number of findings have been reported, supporting their cancer inhibitory effects, primarily by redirecting APCs to reverse the function of T helper 1 (Th1) responses and CTLs [12] through release of iNOS-dependent NO production [13].

Recently, Marigo, I et al [14] demonstrated that deletion of host iNOS, but not ARG, actually reduced the efficacy of experimental adoptive cell transfer (ACT) in preclinical tumor models. Additionally, they also demonstrated that Tip-DCs (tumor necrosis

factor (TNF) and NOS2-producing inflammatory dendritic cells) play a major role in the antitumor activity of ACT in a CD40-CD40L-dependent manner. Tip-DCs mediate NO production via interaction with CTLs, resulting in enhanced tumor-killing activity through TNF and NO production. These findings suggest the potential role of Tip-DC-activating molecules as a method of cancer immunotherapy.

Recently, a 6-mer hepatitis B virus (HBV)-derived peptide, Poly6 has been reported to exert antiviral effects against HIV-1 by inhibiting p300-mediated acetylation of viral integrase [15]. In this study, the immunotherapeutic potential of Poly6 via its treatments in dendritic cells (DCs) and a mouse tumor -bearing model was explored and primarily its capacity to develop conventional DCs into Tip-DCs and its underlying antitumor mechanisms were elucidated.

MATERIALS AND METHODS

1. Ethics statement

All animal experiments were humanely handled and were conducted in compliance with the guidelines approved by the Institutional Animal Care and Use Committee of Seoul National University.

2. Mice

Six-week-old female C57BL/6 mice, Balb nu/nu mice and IFNAR1 knock out mice were purchased from Orient Bio and maintained in a specific pathogen-free (SPF) environment. All procedures were approved in advance by the Institutional Animal Care and Use Committee of Seoul National University (SNU-181010-2).

3. Cells and cell culture

Murine colon cancer cells which were engineered to express human carcinoembryonic antigen (MC38/CEA), murine breast cancer (EO771), murine pancreatic cancer (PanO2), and HBV W4P large surface protein-expressing NIH-3T3 cells (W4P-LHB-NIH3T3) [18] were cultured in Dulbecco's modified Eagle's medium

(DMEM), and human breast cancer (MCF-7, MDA231), mouse melanoma (B16F10), and DC2.4 cells were cultured in Roswell Park Memorial Institute 1640 Medium (RPMI). These media were supplemented with 10% fetal bovine serum (FBS), 100 U/mL penicillin, and 100 μg/mL streptomycin in a 5% CO_2 and 37° C incubator.

4. Preparation of Mouse Bone marrow-derived dendritic cells(BMDCs)

Bone marrow-derived dendritic cells (BMDCs) were harvested from the bone marrow of 7-week-old C57BL/6 mice and were differentiated for 5 days in Iscove's Modified Dulbecco's Medium (IMDM) supplemented with recombinant mouse GM-CSF (20 ng/ml), mouse IL-4 (20 ng/ml), 10% FBS, penicillin (100 U/mL), streptomycin (100 μg/ml), gentamicin (50 μg/ml), L-glutamine (2 mM), and β-mercaptoethanol (50 nM) [18]

5. Tumorigenesis studies

MC38 colon cancer cells engineered to express human carcinoembryonic antigen (CEA) (1×10^6/100 μl), B16F10 melanoma cancer cells (1×10^6/100 μl) and PanO2 pancreatic cancer cells (1×10^6/100 μl) were subcutaneously injected into the right

flank of mice. In this study, All MC38 cell refers to MC38/CEA cancer cell. The Poly6 peptide (10 μg/100 μl) was subcutaneously injected separately from the tumor injection site. For the combined therapeutic effect, anti-PD-L1 (100 μg/100 μl) was intraperitoneally administered. In the nude mouse experiments, W4P-LHB-NIH3T3 cells (1×10^8 cells/100 μl) were subcutaneously injected, and cisplatin (50 μg/100 μl) was peritumorally injected as previously described [18]. To prove inhibition effect of NO in anticancer effect of Poly6 in mouse model, L-NAME (2mg/100 μl) was administrated intravenously 3 times before MC38 cells inoculation. Also, post cancer inoculation, L-NAME was treated 3 times more. Tumor mass was measured and calculated with the following formula: width*width*length*0.52. All mice were sacrificed by CO_2 asphyxiation, and then each tissue was dissected for subsequent experiments.

6. Histopathological study

Fixed tumor tissues were embedded in paraffin and sectioned to a thickness of 5 μm. Sectioned slides were stained with hematoxylin and eosin (H&E). Slides were analyzed with the Aperio Scanscope (Leica Microsystems), and quantification of stained antigens was analyzed using HistoQuest (TissueGnostics).

Apoptotic cell death in tumor tissues was detected by the terminal deoxynucleotidyl transferase-mediated dUTP nick-end labeling (TUNEL) assay using the ApopTag Peroxidase In Situ Apoptosis Detection Kit (Millipore). Stained apoptotic cells were digitalized by the Aperio Scanscope and HistoQuest.

7. Flow cytometry

Tumors were dissociated with collagenase IV (200 U/ml, Sigma) and DNase I (200 μg/ml, Sigma) at 37° C for 30 min with shaking. For flow cytometry, cells were blocked with CD16/32 (Biolegend, 101301). For intracellular cytokine staining, cells were fixed in 1% paraformaldehyde in PBS and permeabilized using 0.1% Triton X-100 in FACS buffer containing 10% FBS and 10 mM EDTA in PBS for 20 min. The following antibodies were used: anti-CD3 (17A2), anti-CD4 (RM4-5), anti-CD8 (53-6.7), anti-CD11b (M1/70), anti-CD11c (HL3), anti-CD40 (3/23), anti-CD80(B7-1), anti-CD86 (GL-1), anti-CD44 (IM7), anti-CD25(3C7), anti-TNF-α (MP6-XT22), anti-iNOS (CXNFT), anti-IFN-γ (XMG1.2), and 3-nitrotyrosine (39B6) [19]. All antibodies were purchased from, Biolegend, BD Bioscience and eBioscience.

8. Analysis of mRNA by real-time PCR

Total mRNA was extracted from tumor tissues and cells using TRIzol reagent and was quantified. Relative expression levels were determined using the SYBR green kit (Bioline, 74005). Primers sequences are shown in Table 1.

Table 1. Primers sequences used in qRT-PCR

Genes		Sequence (5' to 3')
m FasL	Forward	CGGTGGTATTTTTCATGGTTCTGG
	Reverse	CTTGTGGTTTAGGGGCTGGTTGTT
m TRAIL	Forward	CCTCTCGGAAAGGGCATTC
	Reverse	TCCTGCTCGATGACCAGCT
m Fas	Forward	TCTGGTGCTTGCTGGCTCAC
	Reverse	CCATAGGCGATTTCTGGGAC
m Bak	Forward	TCTGGCCCTACACGTCTACC
	Reverse	ACAAACTGGCCCAACAGA AC
m Bax	Forward	GGAGCAGCTTGGGAGCG
	Reverse	AAAAGGCCCCTGTCTTCATGA
m Bcl2	Forward	ACTTCGCAGAGATGTCCAGTCA
	Reverse	TGGCAAAGCGTCCCCTC
m perforin	Forward	CTGGCTCCCACTCCAAGGTA
	Reverse	GGCTGTAAGHACCGAGATGC
m granzymeB	Forward	CCACTCTCGACCCTACATGG
	Reverse	GGCCCCCAAAGTGACATTTATT
m 18s	Forward	AGTCCCTGCCCTTTGTACACA
	Reverse	CGATCCGAGGGCCTCACTA
m mt.Dloop-1	forward	AATCTACCATCCTCCGTGAAACC
	reverse	TCAGTTTAGCTACCCCCAAGTTTAA
m mt.Dloop-2	forward	CCCTTCCCCATTTGGTCT
	reverse	TGGTTTCACGGAGGATGG
m mt.ND4	forward	AACGGATCCACAGCCGTA
	reverse	AGTCCTCGGGCCATGATT

9. Western Blot

Harvested cells were lysed using RIPA buffer (CST, #9806) with phosphate inhibitor and protease inhibitor (Hoffmann-La Roche Inc.). After protein quantification by Bradford assay and denaturation by boiling, protein samples were separated by electrophoresis, transferred to NC membranes, and blocked for 1 hr. Membranes were incubated overnight at 4℃ with primary antibodies (1:1,000). Primary antibodies used were as follows: P300 (sc-8981), NOS2 (sc-4271), cGAS (CST, #31659), and STING (CST, #13647). The next day, membranes were incubated with HRP-conjugated secondary antibodies (1:2,000) for 2 hr. After ECL solution was applied to membranes, proteins were detected on an LAS 2000 imager.

10. Immunofluorescence

Cells were seeded into two-chamber glass slides (Nunc, Roskilde, Denmark). After cells were attached, they were washed with PBS. Cells were incubated in RPMI containing 1% FBS in the presence of PBS, LPS, or Poly6 for 12 hr. Cells were then fixed in 4% paraformaldehyde solution for 10 min and permeabilized with 0.1% Triton-X 100 for 10 min. Cells were blocked for 1 hr and stained with 3-nitrotyrosine [20] for 10 min. Nuclear staining of

cells was performed with DAPI mounting medium (VECTASHIELD Antifade Mounting Medium, H-1000). Images were obtained using a confocal microscope (Leica STED CW) [21]

11. Cell mediated cytotoxicity

DC2.4 cells were seeded (2.5×10^5 cells) into 96-well microplates and incubated with increasing concentrations of Poly6 for 48 hr. Cancer cells (MC38, B16F10, EO771l, PanO2, MDA231) were stained with CFSE for 10 min. CFSE-labeled cells were cocultured with DC2.4 cells, for which the effector target ratio was 5:1. CFSE-labeled cancer cell death was estimated by 7AAD staining using FACS analysis.

12. Cytokine and nitrate assay

DC2.4 cells were seeded (1×10^6 cells) into 6 well plates for 12 hr. Cells were then starved with opti-MEM for 1 hr. After starvation, cells were cultivated with a gradient of Poly6, PBS, or LPS for 48 hr. Culture supernatants were used to measure cytokine levels. To assess cytokine production by DC2.4 cells, interferon beta and TNF-α were measured using enzyme-linked immunosorbent assay (ELISA, eBioscience) kits. Nitric oxide was measured using a nitrite/nitrate assay kit (Sigma) that was used

according to the manufacturer’s protocol.

13. Dissociation of tumor, lymph nodes and spleen

Tumors and lymph nodes were excised and digested in collagenase IV (200 U/ml, Sigma) and DNase I (200 μg/ml, Sigma) in 1% FBS RPMI media for 30 min at 37° C with shaking. Next, EDTA was added, and the supernatant and cells were filtered through a 70 μm filter. Spleen was excised and filtered through a 70 μm filter as well. After centrifugation at 1500 rpm for 5 min, RBC lysis buffer (Sigma) were added for 3 min. Next, 10% FBS containing RPMI was added and the suspended cells were centrifuged at 1500 rpm for 5 min. Pellets were resuspended in complete 10% FBS containing RPMI [22]

14. Measurement and quantification of oxidative DNA damage

An 8-OHdG competitive ELISA was performed using a commercial 8-OHdG ELISA kit (OxiSelect Oxidative DNA Damage ELISA Kit 8-OHdG Quantitation, Cell Biolabs) according to the manufacturer’s instructions.

15. Detection of mitochondrial ROS

Cells were stained with mitoSOX, which is a mitochondrial

superoxide indicator (Invitrogen) to evaluate mitochondrial ROS. Cells were cultured in 96-well flat bottom plates for FACS analysis, and on 2-chamber glass slides (Nunc, Roskilde, Denmark) for immunofluorescence. Adherent cells were stimulated by PBS (control) or Poly6 (10 μM). Stimulated cells were stained with mitoSOX for 20 min at 37℃. MitoSOX intensity levels in cells were measured by FACS and confocal microscopy.

16. Detection of cytosolic mitochondrial DNA

Cells were stimulated with Poly6 for 24 hr. The cytosolic fraction was isolated using the Qproteome Cell Compartment Kit (Qiagen) according to the manufacturer's protocol. Cell pellets were resuspended in 4℃ PBS and centrifuged at 500 *g* for 10 min. The supernatant was removed and pellets were resuspended in protease inhibitor solution-containing lysis buffer and then incubated at 4℃ for 10 min. Lysates were centrifuged at 1000 *g* for 10 min. After centrifugation, supernatants were transferred to new tubes. Supernatants were subjected to the PCI method to extract DNA. Mitochondrial DNA was detected using primer sets that are listed in Table 1.

17. Statistical analysis

Statistical comparison of results was performed by t-test, as well as one and two-way ANOVA. Data are shown as the mean ± standard error of mean (SEM) and were analyzed using Graph Pad Prism version 8.0 (Graph Pad, La Jolla, CA, USA). Statistical significance is denoted with asterisks as follows: * $p \leq 0.05$; ** $p \leq 0.01$; *** $p \leq 0.001$; and **** $p \leq 0.0001$.

RESULTS

1. Poly6 treatment leads to Tip-DC development from DCs in an IFN-I-dependent manner by evoking mitochondrial ROS-mediated cytosolic release of oxidized mitochondrial DNA.

Previously, Poly6, an HBV-derived peptide(Fig. 1A) was introduced that induced antiviral effects against HIV-1 by inhibiting acetylation of HIV-I integrase by downregulation p300 [15]. First, First, Poly6 inhibits p300 expression in DC2.4 cells (Fig. 1B). This led us to hypothesize that DC modulation by Poly6 may lead to the development of conventional DCs into Tip-DCs in an IFN-I-dependent manner because higher IFN-β production is known to be a signature of Tip-DCs [16, 17]. Given that p300 inhibition can affect the mitochondria stress response [23, 24], next the effect of Poly6 treatment on DC activation or maturation were explored. Data showed that Poly6 treatment induced DC maturation in the BMDCs, with expression of maturation markers, including C40, CD80, CD86 or MHC II, increasing (Fig. 1C). In the DC2.4 cell line, similar trend was observed (Fig. 1D). Also, Poly6 treatment leads to mitochondria ROS (mt ROS) production (Fig. 2A, 2B), resulting in cytosolic release of oxidized mitochondrial DNAs (mt DNA) in DC2.4 cells (Fig. 2C, 2D). Oxidized mt DNA can lead to IFN-I

production via the cGAS-Sting axis [21, 25, 26], and treatment with Poly6 can lead to enhanced expression of both cGAS and STING in DC2.4 cells (Fig. 3A). Data indicated that Poly6 leads to enhanced IFN-I production in DCs in a dose-dependent manner (Fig. 3B). Next, the role of increased IFN-I production in Tip-DC development was explored. Poly6 treatment enhanced production of TNF-α (Fig. 3C) and iNOS-dependent NO productions in BMDCs from wild type mice but not from IFNAR1 KO mice (Fig. 3D, 3E). Moreover, Poly6 treatment induced development of BMDCs into Tip-DC in a dose-dependent manner from wild type mice but not from IFNAR1 KO mice (Fig 3F). These data suggest that Poly6 leads to Tip-DC development in a mitochondrial stress-mediated IFN-I-dependent manner via activation of the cGAS-STING axis.

(A)

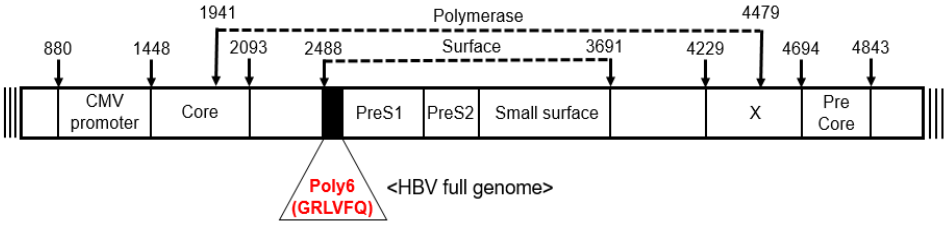
1941
Polymerase
4479
880
1448
2093
2488
Surface
3691
4229
4694
4843
CMV promoter
Core
PreS1
PreS2
Small surface
X
Pre Core
Poly6 (GRLVFQ)
<HBV full genome>

(B)

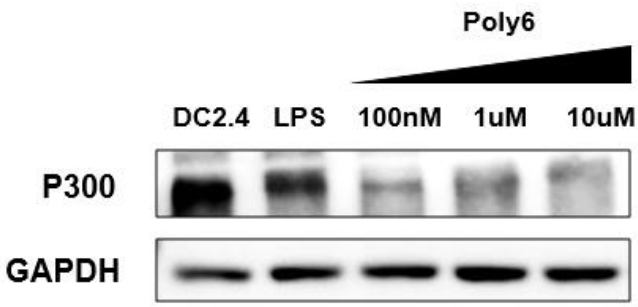
Poly6
DC2.4
LPS
100nM
1uM
10uM
P300
GAPDH

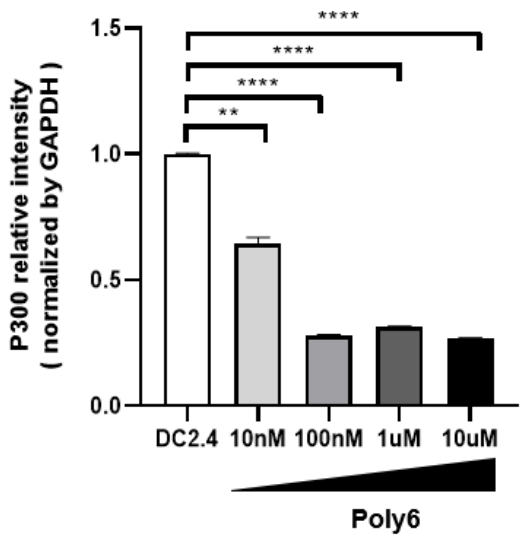
****
****
****
**
1.5
1.0
0.5
0.0
P300 relative intensity (normalized by GAPDH)
DC2.4
10nM
100nM
1uM
10uM
Poly6

(C)

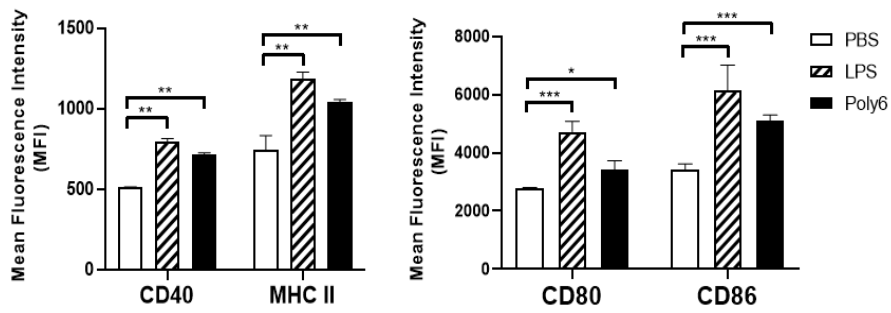

(D)

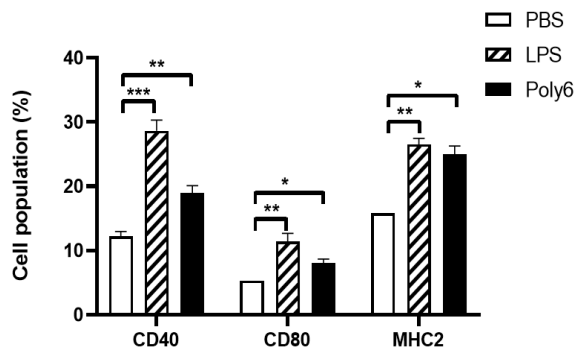

Figure 1. HBV-derived peptide, Poly6 induces maturation of dendritic cells.

(A) schematic Poly6 (GRLVFQ) position figure. Poly6 is a short polypeptide from nucleotide-deleted sequences in the preS1 start region in chronic patients with genotype C2 infection. (B) DC2.4 cells were incubated with Poly6 for 24 hr. P300 protein levels were evaluated by western blotting. (C) BMDCs were starved with opti-MEM media for 30 min and Poly6 (1 μM) was administered for 24 hr. Lipopolysaccharide (LPS) (1 mg/ml) was used as a positive

control. After stimulation with Poly6, maturation of BMDCs was observed by flow cytometry analysis. (D) DC2.4 cells were treated Poly6 (10 μM) for 24 hr. LPS was used as a positive control. Maturation of DC2.4 cells treated with Poly6 was assessed by flow cytometry. These results are representative of two independent experiments. Significance differences ($^{*}p < 0.05$; $^{**}p < 0.01$; $^{***}p < 0.001$ and $^{****}p < 0.0001$) among different groups are shown in related figures, and the data are presented as the mean ± standard error of mean (SEM); $n = 3$ biologically independent samples. Student's t-test, one- and two-way ANOVA were used.

(A)

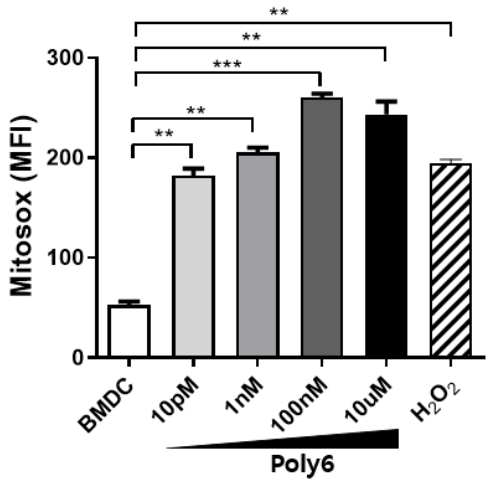
**
**
***
**
**
300
200
100
0
Mitosox (MFI)
BMDC
10pM
1nM
100nM
10uM
H2O2
Poly6

(B)

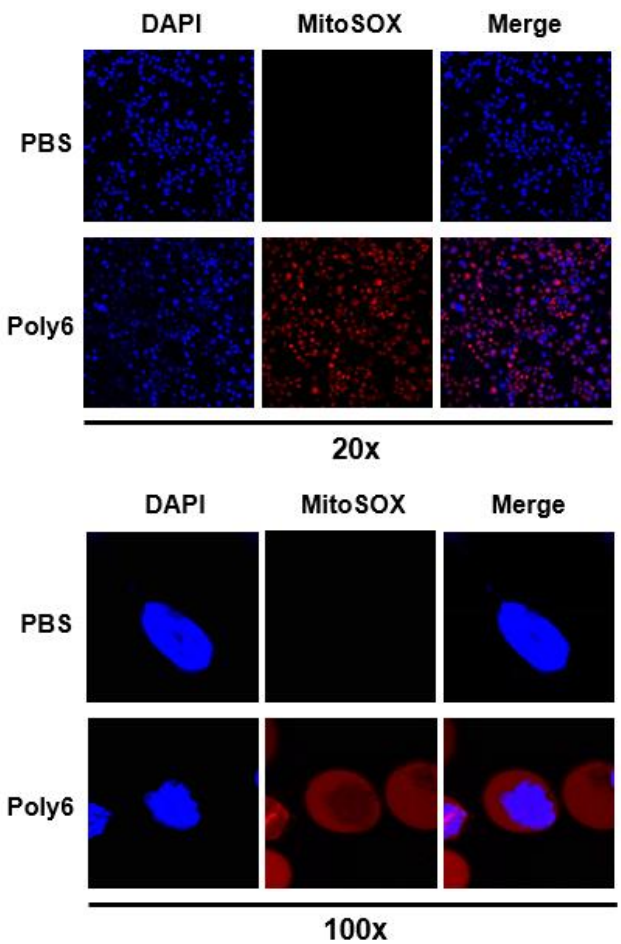
DAPI
MitoSOX
Merge
PBS
Poly6
20x
DAPI
MitoSOX
Merge
PBS
Poly6
100x

(C)

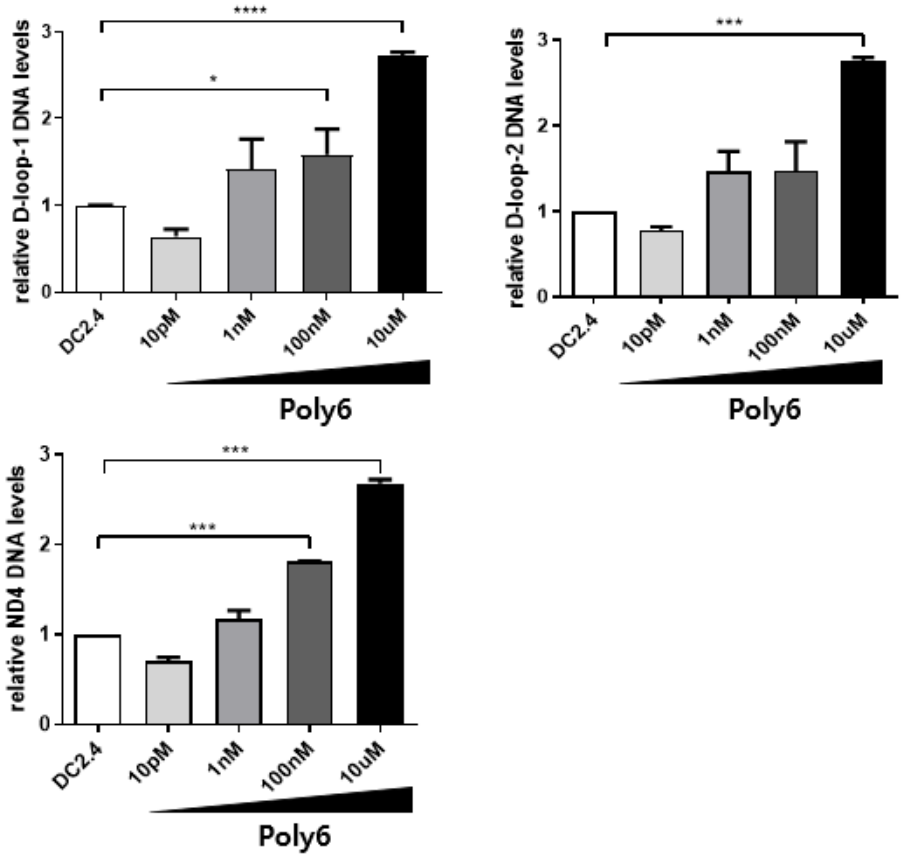
relative D-loop-1 DNA levels
****
*
0
1
2
3
DC2.4
10pM
1nM
100nM
10uM
Poly6
relative D-loop-2 DNA levels
***
0
1
2
3
DC2.4
10pM
1nM
100nM
10uM
Poly6
relative ND4 DNA levels
***
***
0
1
2
3
DC2.4
10pM
1nM
100nM
10uM
Poly6

(D)

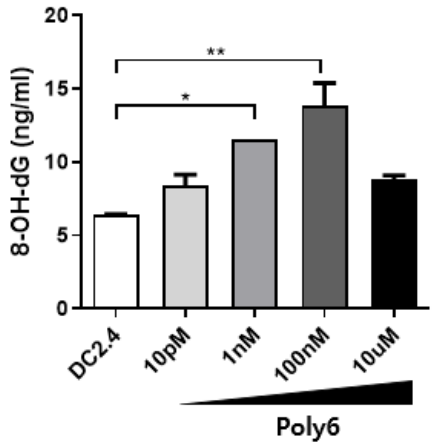
8-OH-dG (ng/ml)
**
*
0
5
10
15
20
DC2.4
10pM
1nM
100nM
10uM
Poly6

Figure 2. Poly6 evokes mtROS-mediated cytosol release of oxidized mtDNA.

(A) To evaluate mitochondrial ROS, BMDCs were stimulated with Poly6 for 12 hr. Additionally, cells were treated with H_2O_2 as a positive control. Stimulated cells were stained with MitoSOX (5 μM) and assessed by FACS. (B) DC2.4 cells were incubated with Poly6 (10 μM) for 12 hr. Cells were stained for mitochondrial superoxide (MitoSOX, red) and nuclei (DAPI, blue) and then analyzed using confocal microscopy at 20× and 100× magnification. (C) Cytosolic mt DNA was extracted from nuclear and cytosolic fractions of DC2.4 cells that were treated with Poly6 for 24 hr. Measurement of cytosolic mt DNA expression by qRT-PCR using the mitochondrial D-loop-1, D-loop-2 and ND4 primer sets. (D) Cytosolic DNA was obtained from Poly6 stimulated DC2.4 cells, and levels of 8-OHdG were measured using an ELISA kit. These results are representative of two independent experiments. Significance differences ($^{*}p < 0.05$; $^{**}p < 0.01$; $^{***}p < 0.001$ and $^{****}p < 0.0001$) among different groups are shown in related figures, and the data are presented as the mean ± standard error of mean (SEM); $n=3$ biologically independent samples. Student's t-test, one- and two-way ANOVA were used.

(A)

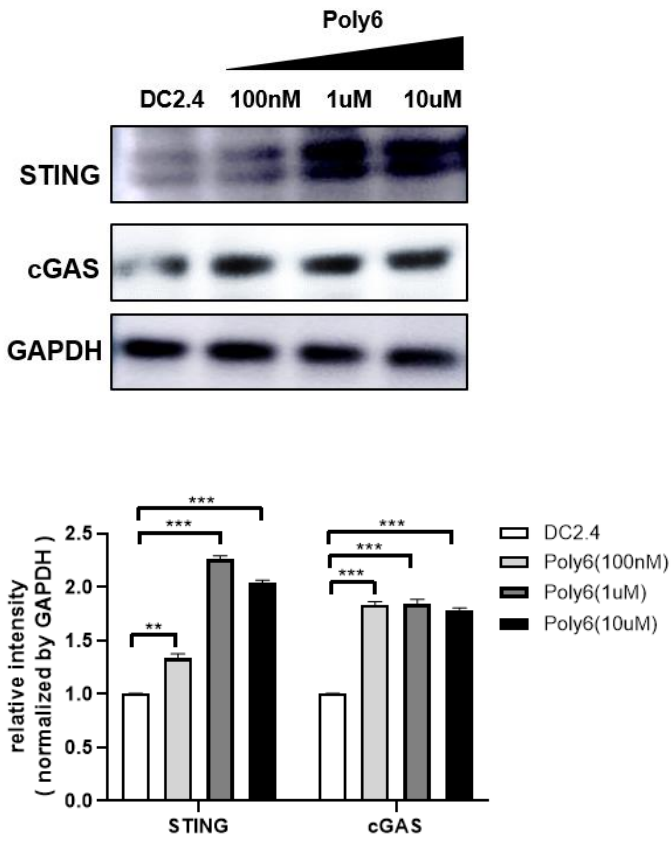
Poly6
DC2.4
100nM
1uM
10uM
STING
cGAS
GAPDH
relative intensity
(normalized by GAPDH)
2.5
2.0
1.5
1.0
0.5
0.0
**
***
***
***
***
***
STING
cGAS
DC2.4
Poly6(100nM)
Poly6(1uM)
Poly6(10uM)

(B)

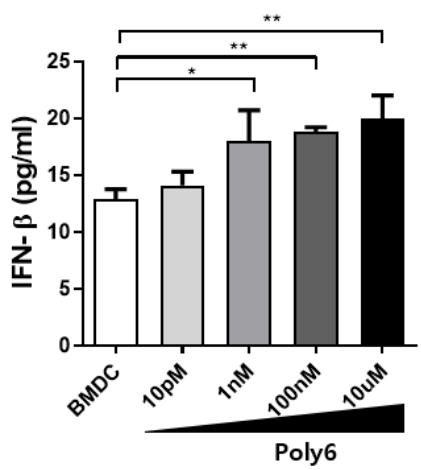
IFN-β (pg/ml)
25
20
15
10
5
0
*
**
**
BMDC
10pM
1nM
100nM
10uM
Poly6

(C)

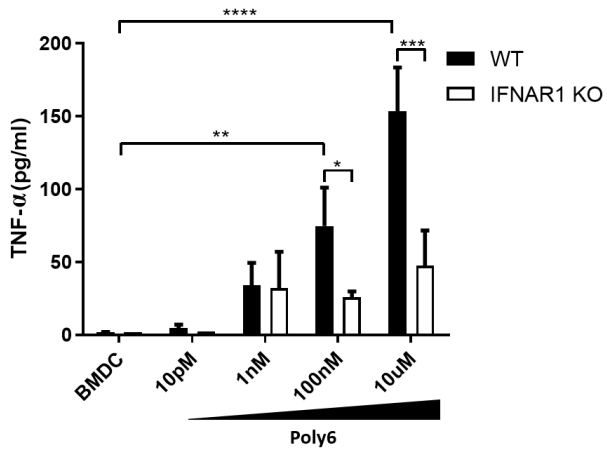
****
***
**
*
200
150
100
50
0
TNF-α(pg/ml)
WT
IFNAR1 KO
BMDC
10pM
1nM
100nM
10uM
Poly6

(D)

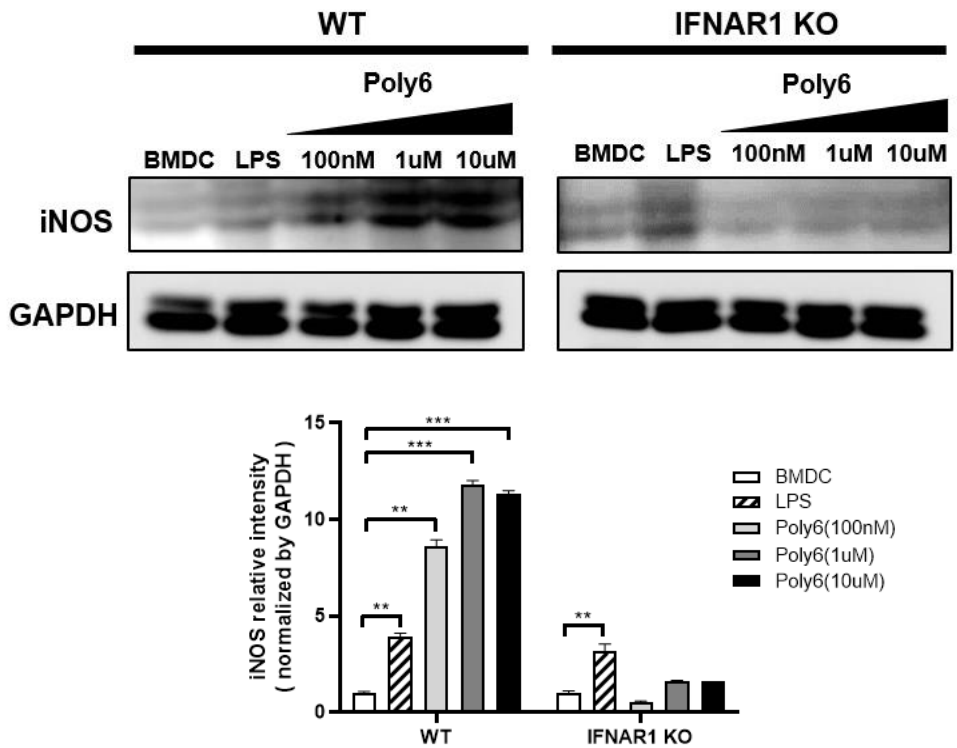
WT
IFNAR1 KO
Poly6
Poly6
BMDC LPS 100nM 1uM 10uM
BMDC LPS 100nM 1uM 10uM
iNOS
GAPDH
15
10
5
0
iNOS relative intensity
(normalized by GAPDH)
***
***
**
**
**
BMDC
LPS
Poly6(100nM)
Poly6(1uM)
Poly6(10uM)
WT
IFNAR1 KO

(E)

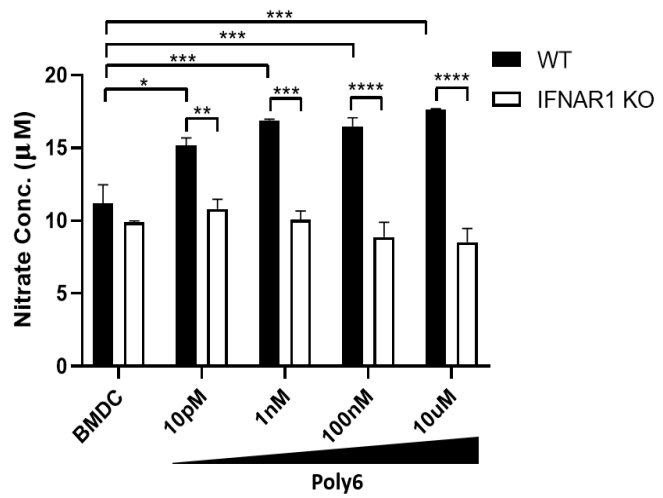

(F)

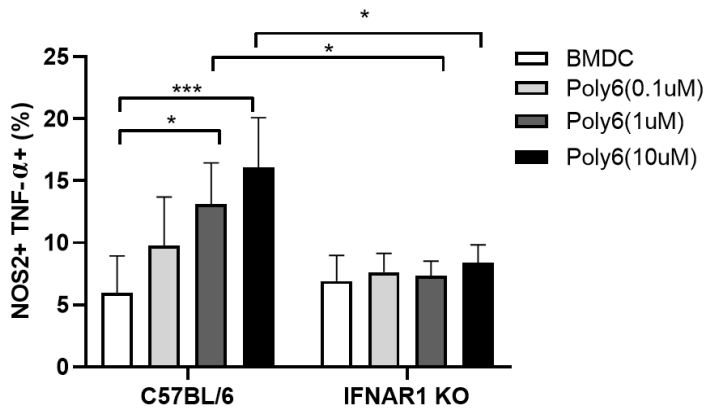

Figure 3. Poly6 treatment leads to development of Tip-DCs from DCs in an IFN-I-dependent manner.

(A) STING and cGAS protein levels were assessed by western blotting assay and detected by LAS 2000. (B) Supernatants of stimulated BMDCs were collected, and IFN-β ELISA was used for

measuring Type I IFN levels. (C) Supernatants of stimulated BMDCs from WT and IFNAR1 KO mice were collected, and TNF-α levels were measured by TNF-α ELISA. (D) BMDCs from wild type C57BL/6 mice and IFNAR1 KO mice were differentiated and exposed to Poly6 stimulation. NOS2 protein was analyzed by western blotting. (E) For detection of nitric oxide metabolites, nitrate concentration was assessed by nitrite/nitrate assay kit. (F) Development of Poly6 treated BMDCs into Tip-DCs from WT and IFNAR1 KO mice was analyzed by flow cytometry. These results are representative of two independent experiments. Significance differences ($^{*}p < 0.05$; $^{**}p < 0.01$; $^{***}p < 0.001$ and $^{****}p < 0.0001$) among different groups are shown in related figures, and the data are presented as the mean ± standard error of mean (SEM); $n=3$ biologically independent samples. Student's t-test, one- and two-way ANOVA were used.

2. Poly6 exerts anticancer effects in an IFN-I dependent manner in mouse models.

Next, investigation was conducted whether Poly6, capable of inducing Tip-DC and DC maturation in an IFN-I-dependent manner, also had potential as an anticancer vaccine. Therefore, the anticancer potential of Poly6 was evaluated in C57BL/6 mice injected with MC38 mouse colon cancer and B16F10 mouse melanoma cancer. To evaluate the therapeutic effects of Poly6, MC38 (1×10^6/100 μl) cells were subcutaneously injected into right side of mice on day 0 and Poly6 (10 μg) was subcutaneously introduced 3 times on days 1, 3 and 5 after cancer injection (Fig. 4A). These data showed that Poly6 significantly inhibited cancer growth and weight of tumor tissues compared to the PBS group (Fig. 4B, 4C, 4D). H&E staining showed reduction of tumor density and induced recruitment of tumor infiltrating lymphocytes in Poly6 treated mice compared to PBS treated mice (Fig. 4E). A similar anticancer effect of Poly6 was also observed in a mouse xenograft model implanted with B16F10 mouse melanoma cancer (Fig. 5B, 5C, 5D) following an experimental schedule (Fig. 5A). Also, anticancer trend was found in PanO2 mouse pancreatic cancer -bearing model (Fig. 5E, 5F, 5G, 5H). Furthermore, the anticancer effect of Poly6 in another MC38-bearing model was

explored. In this model, Poly6 was presented prior to cancer cell seeding (1 day prior to cancer injection) via a subcutaneous route for pre-activation of DCs and further challenged 3 times at longer time intervals: on days 7, 14 and 24 after cancer injection (Fig. 6A). In this model, Poly6 treated mice also exhibited reduction of tumor size and weight as shown in the therapeutic effect model (Fig. 6B, 6C, 6D). In addition, tumor incidence was markedly reduced and mouse survival was significantly increased in Poly6 challenged mice compared to the PBS group (Fig. 6E, 6F). Next, IFN-I dependency of the anticancer effect of Poly6 was checked by comparing the anticancer effects of Poly6 treatment between wild type and IFN-KO mice (Fig. 7A). The reduction of tumor mass and weight by Poly6 observed in WT mice was not found in IFN KO mice (Fig. 7B, 7C, 7D). These results suggest that Poly6 has anticancer therapeutic potential in an IFN-I dependent manner in cancer -bearing mouse models.

(A)

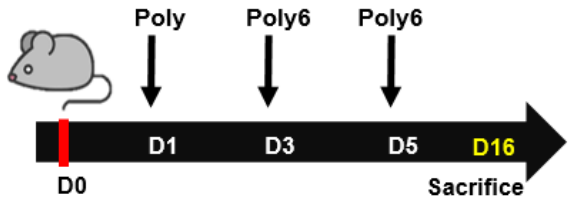
Poly
Poly6
Poly6
D1
D3
D5
D16
D0
Sacrifice

(B)

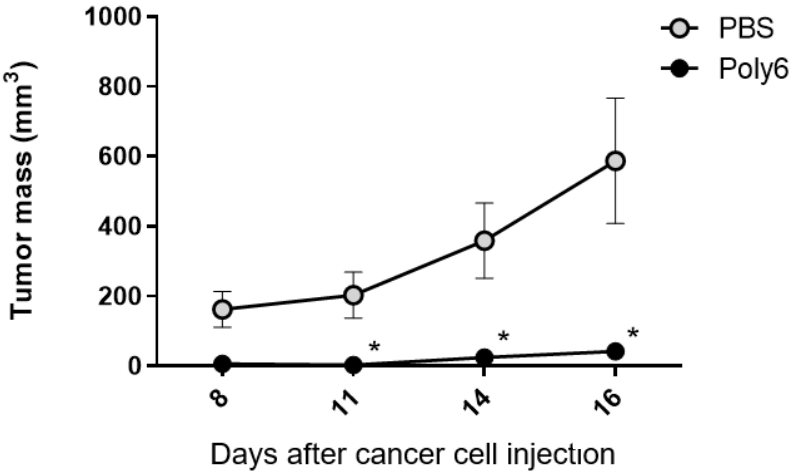
Tumor mass (mm3)
1000
800
600
400
200
0
PBS
Poly6
*
*
*
8
11
14
16
Days after cancer cell injection

(C)

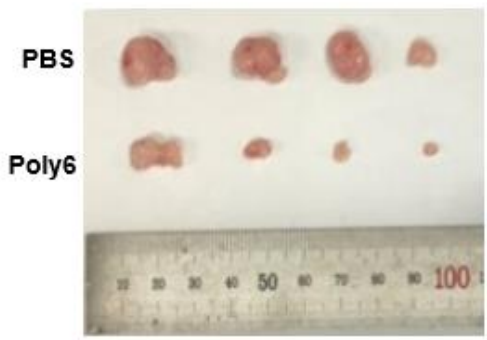
PBS
Poly6

(D)

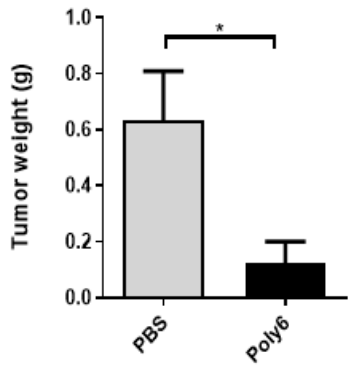
Tumor weight (g)
1.0
0.8
0.6
0.4
0.2
0.0
*
PBS
Poly6

(E)

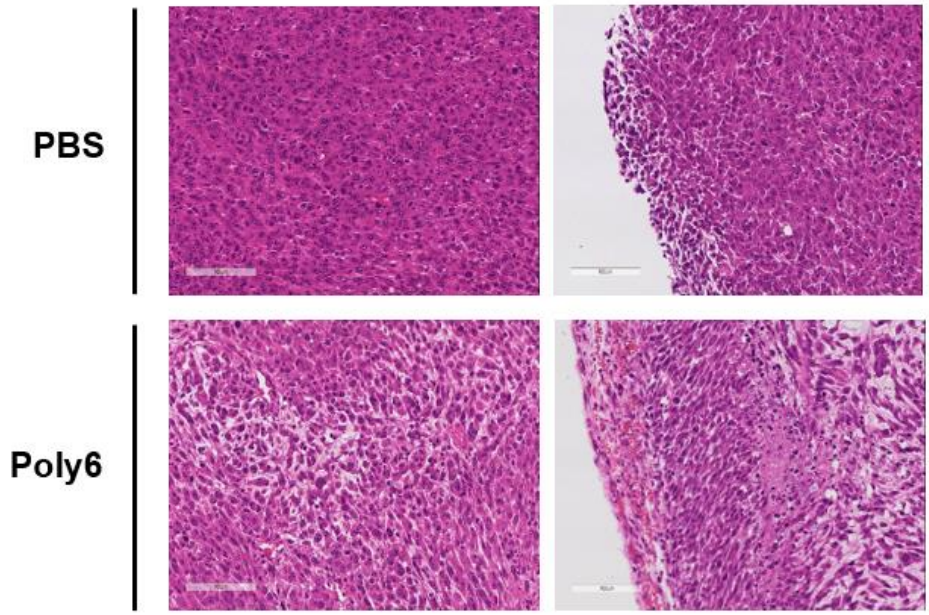

Figure 4. Poly6 exerts an anticancer effect in a colon cancer mouse model.

(A) Schematic in vivo experimental schedule performed post treatment with Poly6 to verify its therapeutic anticancer effect. MC38 cells ($1 \times 10^6/100\,\mu l$) were inoculated by subcutaneous route into C57BL/6 mice (n=4). (B) Observation of attenuated tumor progression by assessing MC38 tumor growth. (C) Images of tumors extracted from MC38 tumor-bearing mice on day 16. (D) MC38 colon tumor weight was calculated. (E) H&E staining of tumors extracted from MC38 tumor-bearing mice. Tumor mass was calculated using the following formula: width* width*length*0.52, and mice with over 1000 mm^3 of tumor mass

were sacrificed by CO_2 asphyxiation. These results are representative of two independent experiments. Significance differences ($^{*}p < 0.05$; $^{**}p < 0.01$; $^{***}p < 0.001$ and $^{****}p < 0.0001$) among different groups are shown in related figures, and The data are presented as the mean ± standard error of mean (SEM) of the mice. Student's t-test, one- and two-way ANOVA were used.

(A)

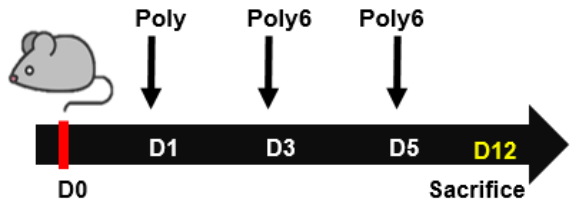
Poly
Poly6
Poly6
D1
D3
D5
D12
D0
Sacrifice

(B)

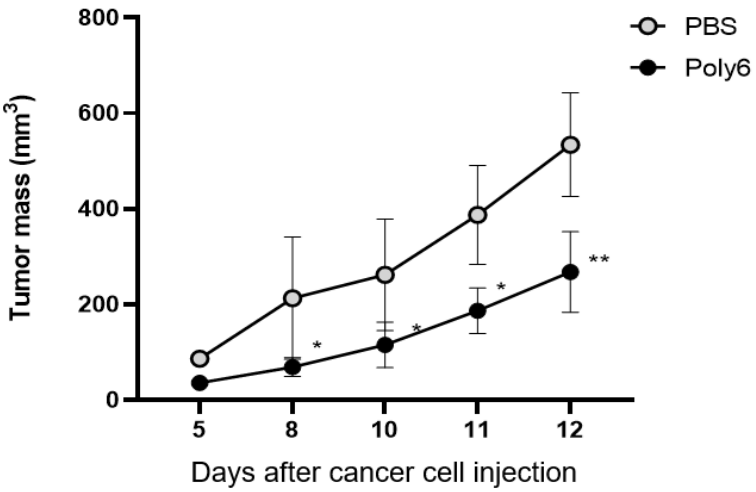
800
600
400
200
0
Tumor mass (mm3)
PBS
Poly6
5
8
10
11
12
Days after cancer cell injection
*
*
*
**

(C)

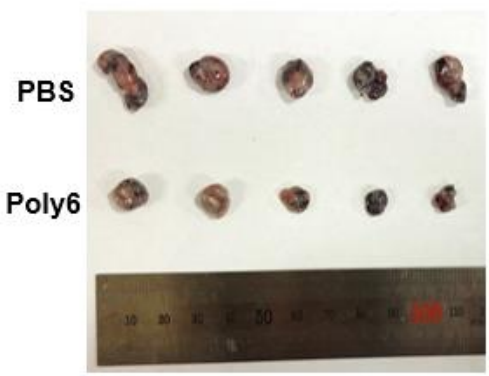
PBS
Poly6

(D)

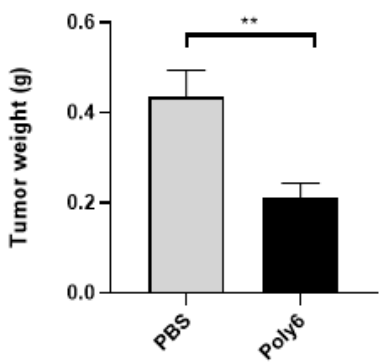
0.6
0.4
0.2
0.0
Tumor weight (g)
**
PBS
Poly6

(E)

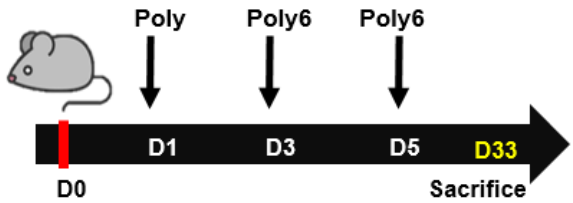
Poly
Poly6
Poly6
D1
D3
D5
D33
D0
Sacrifice

(F)

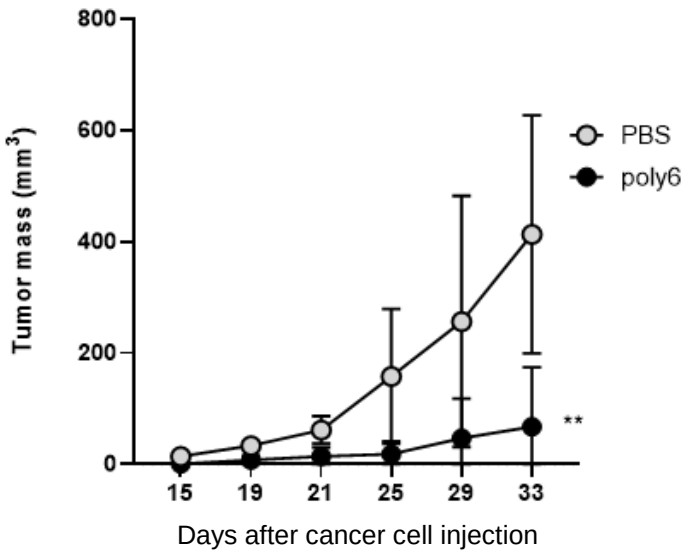
800
600
400
200
0
Tumor mass (mm3)
PBS
poly6
**
15
19
21
25
29
33
Days after cancer cell injection

(G)


PBS
Poly6

(H)

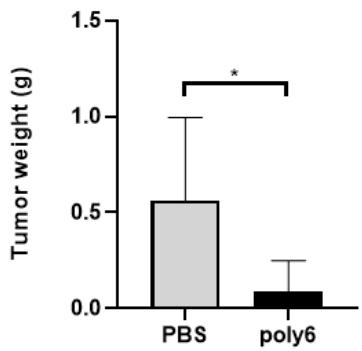
1.5
1.0
0.5
0.0
Tumor weight (g)
*
PBS
poly6

Figure 5. Poly6 exerts anticancer effects in a melanoma and a pancreatic cancer-bearing mouse model.

(A) *in vivo* experimental schedule of melanoma cancer. B16F10 cells (1×10^6) were subcutaneously injected into C57BL/6 mice (n=5). **(B)** Tumor growth in melanoma tumor. **(C)** Image of B16F10 tumor on day 12. **(D)** Weight of B16F10 tumor tissues was calculated. **(E)** *in vivo* schedule of pancreatic cancer model. PanO2 cells were inoculated on day 0, and then Poly6(10ug) was administrated 3 times. (n=4) **(F)** Comparison of tumor growth between PBS and Poly6 treated group. **(G)** Picture of tumor tissue. Tumor was not found in half of Poly6 treated mouse. **(H)** Weight of pancreatic tumor tissues. Tumor mass was calculated using the following formula: width* width*length*0.52, and mice with over 1000 mm^3 of tumor mass were sacrificed by CO_2 asphyxiation. These results are representative of two independent experiments. Significance differences ($^{*}p < 0.05$; $^{**}p < 0.01$; $^{***}p < 0.001$ and $^{****}p < 0.0001$) among different groups are shown in related figures, and The data are presented as the mean ± standard error of mean (SEM) of the mice. Student's t-test, one- and two-way ANOVA were used.

(A)

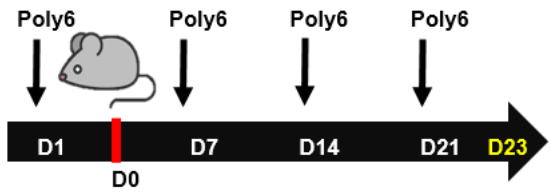
Poly6
Poly6
Poly6
Poly6
D1
D7
D14
D21
D23
D0

(B)

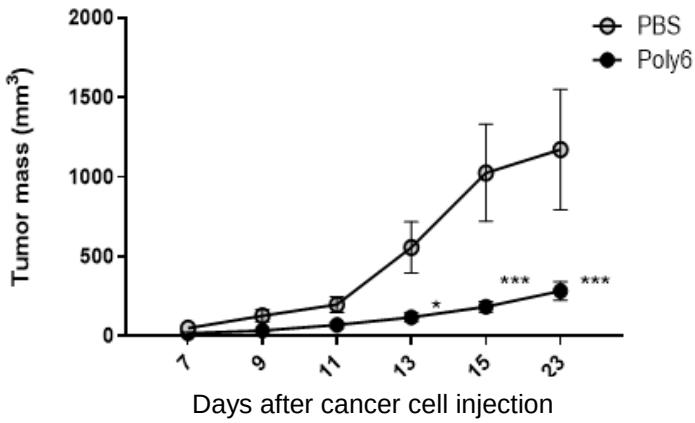
2000
1500
1000
500
0
Tumor mass (mm3)
PBS
Poly6
***
***
*
7
9
11
13
15
23
Days after cancer cell injection

(C)

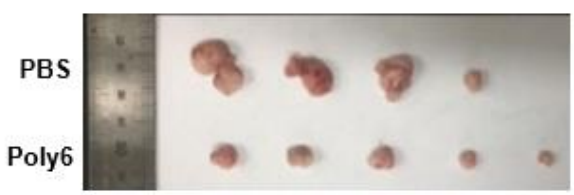
PBS
Poly6

(D)

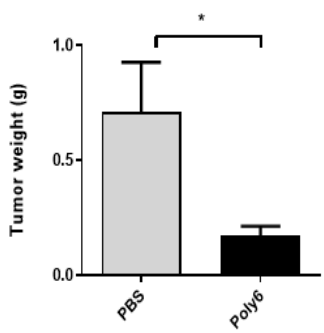
*
1.0
0.5
0.0
Tumor weight (g)
PBS
Poly6

(E)

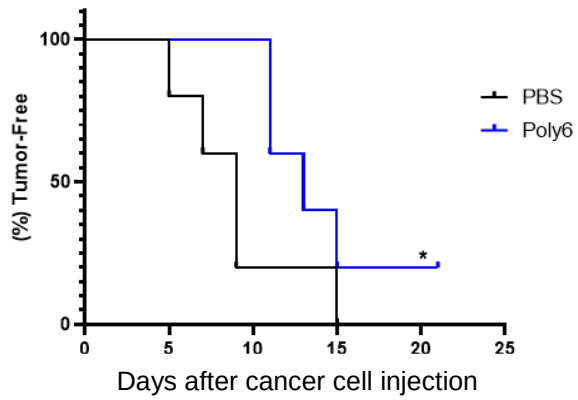

(F)

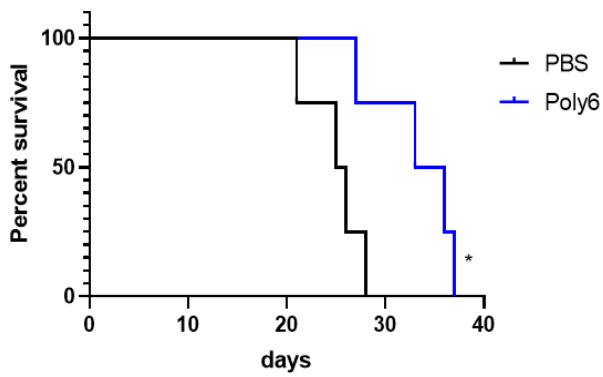

Figure 6. Poly6 exerts anti-cancer effects on pre-activated cancer mouse models and influences tumor incidence and mouse survival. (A) Schematic *in vivo* schedule of pre-activation experiments. Mice were administered Poly6 (10ug/100 μl) before MC38 cancer cell inoculation. The next day, MC38 cells (1×10^6 cells/100 μl) were subcutaneously inoculated into C57BL/6 mice. After cancer cell injection, Poly6 was administered 3 times more times distant from

the site of MC38 injection (PBS; n=4, Poly6; n=5). **(B)** Comparison of tumor growth followed by treatment with Poly6. **(C)** Images of tumors extracted from MC38-bearing mice on day 23. **(D)** Weight of MC38 cancer on day 23. **(E)** Tumor incidence was improved in C57BL/6 mice treated with Poly6 three times after injection of 1×10^6 MC38 cells. The percent of tumor-free mice was indicated (n=5). **(F)** Survival rate was estimated in tumor-bearing mice after Poly6 injection 3 times (n=4). These results are representative of two independent experiments. Significance differences ($^{*}p < 0.05$; $^{**}p < 0.01$; $^{***}p < 0.001$ and $^{****}p < 0.0001$) among different groups are shown in related figures, and the data are presented as the mean ± standard error of mean (SEM) of the mice. Student's t-test, one- and two- way ANOVA were used. Survival test was evaluated by Log-rank test survival analysis.

(A)

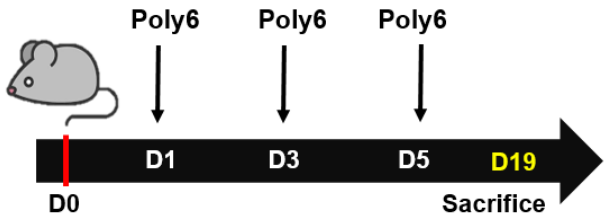
Poly6
Poly6
Poly6
D1
D3
D5
D19
D0
Sacrifice

(B)

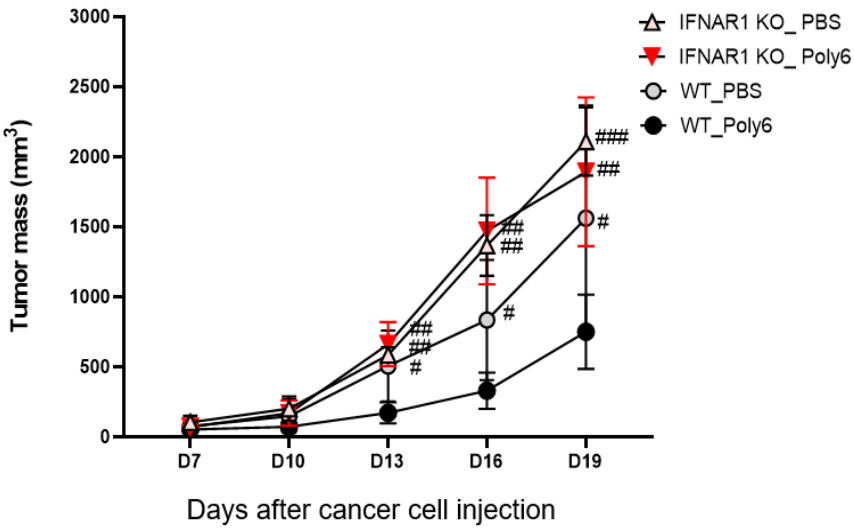
IFNAR1 KO_ PBS
IFNAR1 KO_ Poly6
WT_PBS
WT_Poly6
Tumor mass (mm3)
3000
2500
2000
1500
1000
500
0
D7
D10
D13
D16
D19
Days after cancer cell injection

(C)

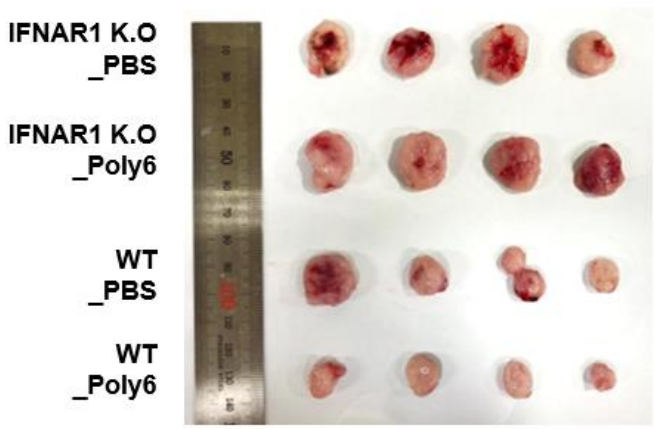
IFNAR1 K.O
_PBS
IFNAR1 K.O
_Poly6
WT
_PBS
WT
_Poly6

(D)

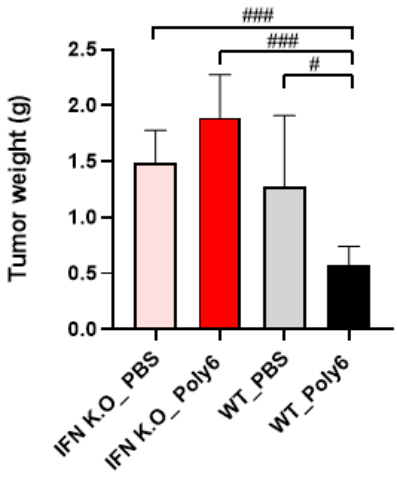

Figure 7. Poly6 exerts anticancer effects in a Type 1 interferon (IFN-I)-dependent manner.

(A) *In vivo* schematic schedule of MC38 injected interferon knock out mouse experimental model (n=4). (B) Tumor growth inhibition by Poly6 in WT C57BL/6 mice but not in IFNAR1 KO mice. (C) Tumor tissue image and (D) weight of WT and IFNAR1 KO mice. Tumor mass was calculated using the following formula: width*width*length*0.52. These results are representative of two independent experiments. Significance differences ($^{\#}p < 0.05$; $^{\#\#}p < 0.01$ and $^{\#\#\#}p < 0.001$) are used to compare with the Poly6-treated wild-type C57BL/6 mouse group. The data are presented as the mean ± standard error of mean (SEM) of the mice. Student's t-test, one- and two-way ANOVA were used.

3. Poly6 exerts anticancer effects via induction of apoptotic tumor cell death in the tumor microenvironment primarily via activating the CD8 T cell-mediated CTL response.

Apoptotic cell death of cancer cells in the tumor microenvironment is one of the major features of successful cancer immunotherapy [27]. To examine whether Poly6 treatment induces apoptosis of cancer cells, tumor sections from xenograft mice were analyzed by TUNEL staining. Data revealed that Poly6 treatment led to increased apoptotic cell death in cancer tissues (Fig. 8A). Furthermore, transcription levels of death signal inducing proteins, Fas, Fas ligand (FasL) and TRAIL, were significantly upregulated in Poly6 treated mice compared to PBS treated mice. In addition, transcription levels of the well-known cytolytic proteins granzyme B and perforin and pro-apoptotic proteins Bax, Bak and cytochrome C were also increased in tumor tissues from Poly6 challenged mice (Fig. 8B).

(A)

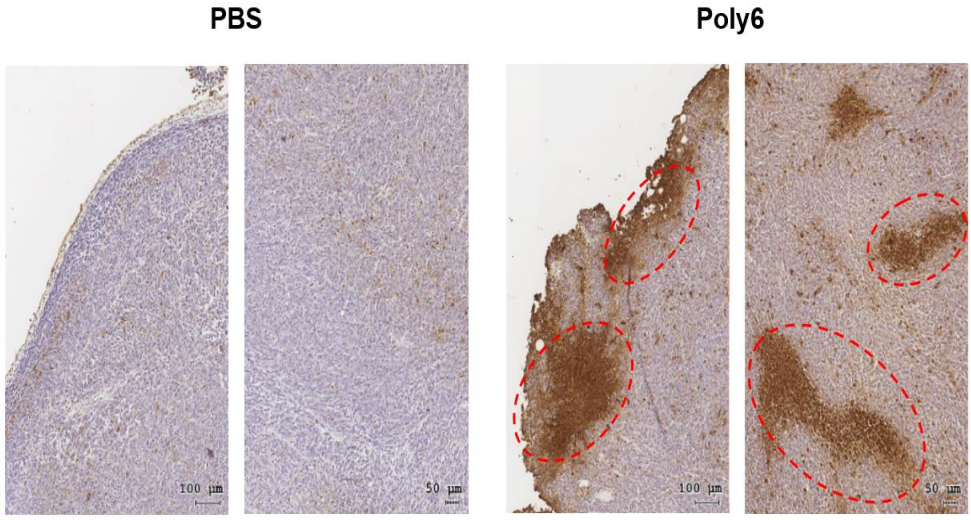
PBS
Poly6
100 μm
50 μm
100 μm
50 μm

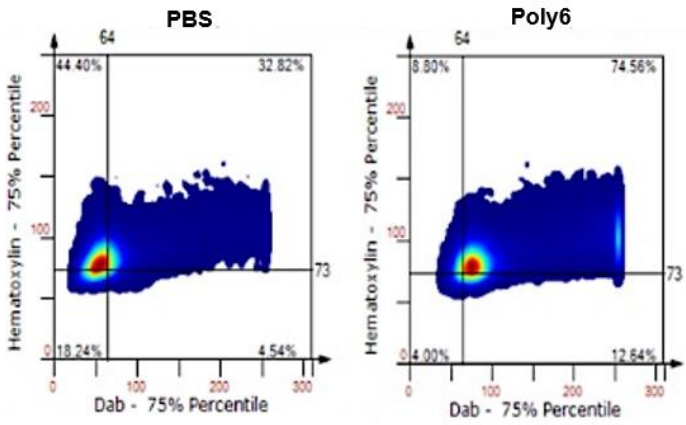
PBS
Poly6
64
44.40%
32.82%
18.24%
4.54%
8.80%
74.56%
4.00%
12.64%
73
Hematoxylin - 75% Percentile
Dab - 75% Percentile
0
100
200
300

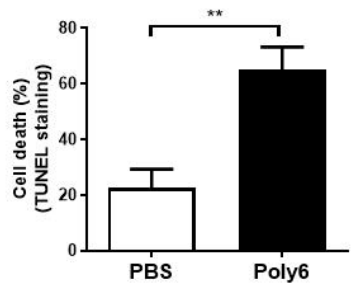
**
Cell death (%)
(TUNEL staining)
80
60
40
20
0
PBS
Poly6

(B)

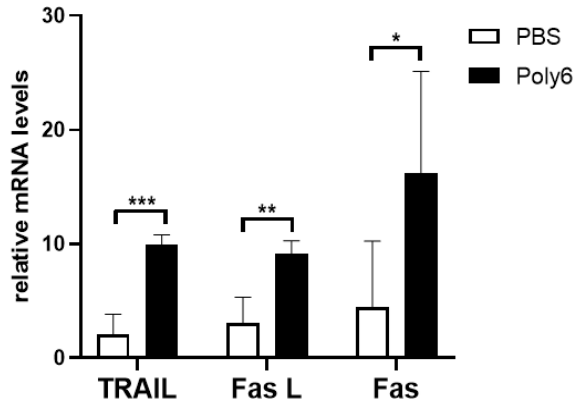
30
20
10
0
relative mRNA levels
PBS
Poly6
***
**
*
TRAIL
Fas L
Fas

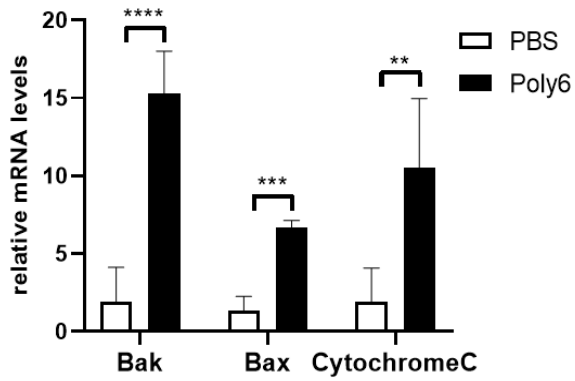
20
15
10
5
0
relative mRNA levels
PBS
Poly6
****
***
**
Bak
Bax
CytochromeC

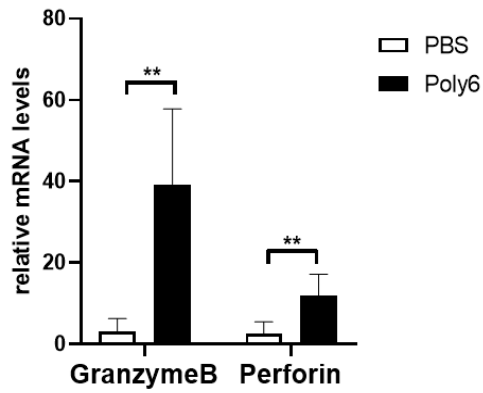
80
60
40
20
0
relative mRNA levels
PBS
Poly6
**
**
GranzymeB
Perforin

Figure 8. Poly6 induces reduction of tumor progression via apoptotic cancer cell death in the tumor microenvironment.

(A) Tumor tissues were extracted on day 19 after MC38 inoculation. Apoptotic cells in MC38 tumor tissue paraffin sections were identified by TUNEL assay, and apoptotic DAB positive cells were quantified by Tissue FAXS analysis. Increased apoptotic cells were indicated by dashed circles. (B) The transcription level of death signal inducing proteins (TRAIL, Fas ligand, Fas), cytolytic proteins (granzyme B, perforin), and pro-apoptotic proteins (Bak, Bax, cytochrome C), in MC38 tumors was assessed by qRT-PCR. These results are representative of two independent experiments. Significance differences ($^{*}p < 0.05$; $^{**}p < 0.01$; $^{***}p < 0.001$ and $^{****}p < 0.0001$) among different groups are related figures, and the data are presented as the mean ± standard error of mean (SEM) of the mice (n = 4). Student's t-test was used.

Next, responsible for CTL of cancer cells, the effect of Poly6 treatment in NK cells or T cell activation was evaluated. In tumor tissue, overall $CD4^+$ and $CD8^+$ T cell populations were increased in tumor regions of Poly6 treated mice (Fig. 9A). Poly6 treatment also significantly increased expression levels of CD44 or CD25, indicative surface markers for activated T cells, on $CD4^+$ and $CD8^+$ T cells in the tumor and spleen (Fig. 9B, 9C). Also, Poly6 treatment increased production of TNF-α or IFN-γ producing CD4 and CD8 T cells in tumor tissue, which are capable of exerting anticancer effector functions (Fig. 9D). However, increased activated T cell populations induced by Poly6 treatment were not found in IFNAR1 KO mice, suggesting that Poly6 leads to enhanced T cell response in an IFN-I-dependent manner (Fig. 9E). The anticancer effects of Poly6 were also observed in melanoma tumor tissue (Fig. 9F). However, Poly6 treatment did not lead to significant increases in activated NK cells, the other cell eliciting CTL response, in the MC38-bearing mouse model (Fig. 9G). Collectively, data suggest that the tumor inhibitory effects found in Poly6 treated mice were attributed to tumor cell apoptotic cell death due to activated CD8 T cell mediated CTL response.

(A)

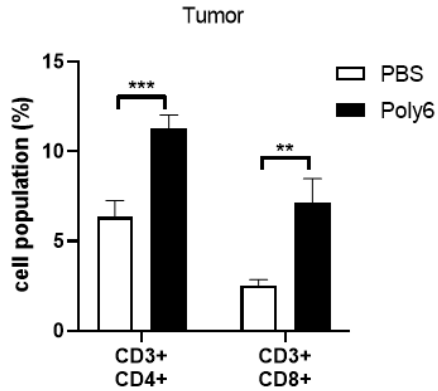
Tumor
PBS
Poly6
cell population (%)
15
10
5
0
***
**
CD3+
CD4+
CD3+
CD8+

(B)

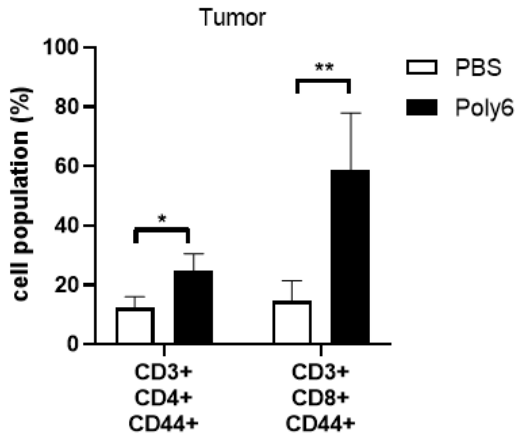
Tumor
PBS
Poly6
cell population (%)
100
80
60
40
20
0
**
*
CD3+
CD4+
CD44+
CD3+
CD8+
CD44+

(C)

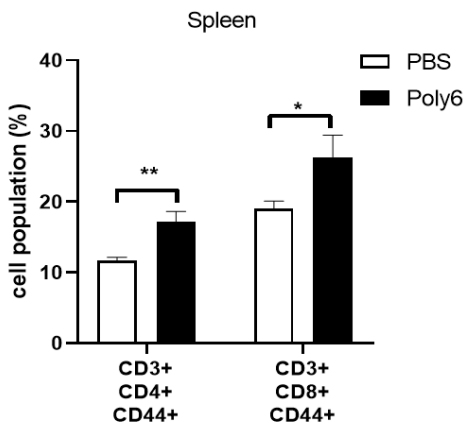
Spleen
PBS
Poly6
cell population (%)
40
30
20
10
0
**
*
CD3+
CD4+
CD44+
CD3+
CD8+
CD44+

(D)

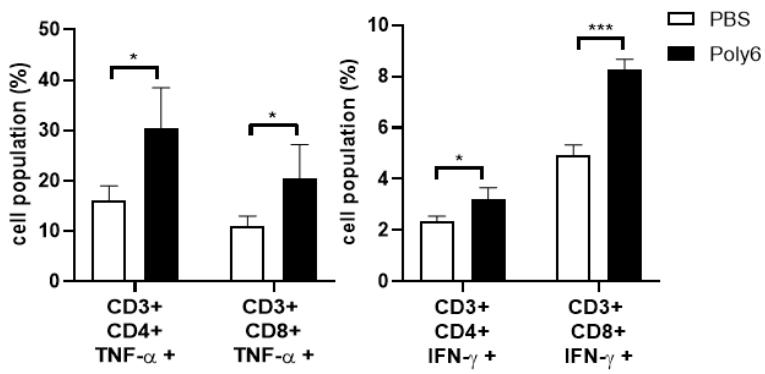
cell population (%)
CD3+ CD4+ TNF-α +
CD3+ CD8+ TNF-α +
CD3+ CD4+ IFN-γ +
CD3+ CD8+ IFN-γ +
PBS
Poly6

(E)

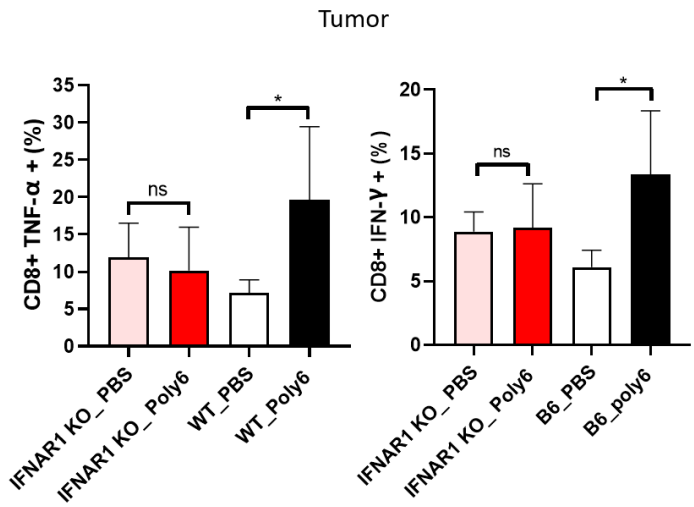
Tumor
CD8+ TNF-α + (%)
CD8+ IFN-γ + (%)
ns
IFNAR1 KO_ PBS
IFNAR1 KO_ Poly6
WT_PBS
WT_Poly6
B6_PBS
B6_poly6

(F)

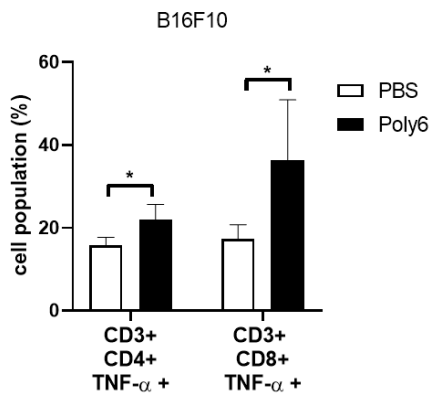
B16F10
cell population (%)
CD3+ CD4+ TNF-α +
CD3+ CD8+ TNF-α +
PBS
Poly6

(G)

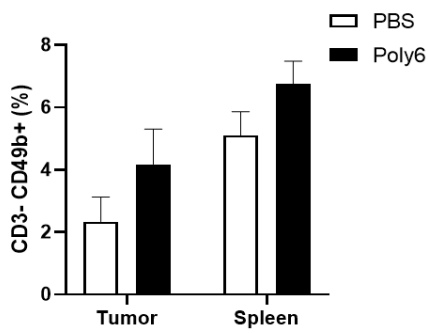
CD3- CD49b+ (%)
Tumor
Spleen
PBS
Poly6

Figure 9. Poly6 induces reduction of tumor progression via induction of T cell activation in the tumor microenvironment.

(A) Evaluation of CD4+ and CD8+ T cells populations in MC38 tumor tissue extracted on day 16. **(B)** Single cells from dissociated MC38 tumor tissues extracted on day 16 after MC38 injection were stained with anti-CD44 surface antibody, and then CD44+ T cells were analyzed using FACS. **(C)** The population of activated CD44+ T cells in splenocytes extracted from MC38 tumor-bearing mice on day 16 was assessed by FACS analysis. **(D)** Populations of TNF-α or IFN-γ producing CD4+ and CD8+ effector T cells in MC38 tumors were analyzed by FACS. **(E)** TNF-α or IFN-γ producing effector CD8+ T cells population in WT and IFNAR1 KO mouse tumor tissues extracted on day 19. **(F)** TNF-α producing effector CD4+ and CD8+ T cells in B16F10 tumor tissue were analyzed by FACS. **(G)** The population of CD3- CD49b+ natural killer cells were analyzed in the MC38 tumor extracted on day 16. Significance differences ($^{*}p < 0.05$; $^{**}p < 0.01$; $^{***}p < 0.001$ and $^{****}p < 0.0001$) among different groups are related figures, and the data are presented as the mean ± standard error of mean (SEM) of the mice. Student's t-test was used.

4. Poly6 induces generation of Tip-DCs and CD40-CD40L activation of DCs.

Since Poly6 treatment was subcutaneously introduced separate from the cancer cell injected site and led to apoptotic cancer cell death primarily due to CD8 T cell mediated CTL response in the tumor microenvironment, hypothesis was established that Poly6 treatment leads to recruitment of activated innate APCs, including macrophages or DCs, into the tumor microenvironment, resulting in activating the cancer-specific CD8 T cell-mediated CTL response. The recruitment of DCs (Fig. 10A), but not macrophages, into tumor sites and the spleen was increased (Fig. 10B), suggesting that DCs may play a major role in inducing cancer-specific T cell responses. Recently, it has been reported that development into Tip-DCs in tumor microenvironments, guaranteeing effective CD8 T cells, mediates tumor rejection via the CD40/CD40L axis [14]. In addition, these data demonstrated that Poly6 treatment, as shown in Fig. 1, leads to enhanced IFN-I production in DCs, resulting in enhanced production of Tip-DC. Interestingly, Poly6 treatment in MC38-bearing mice led to increased population of Tip-DC in the tumor region and spleen using a gating strategy (Fig. 10C, 10D). A similar trend was also observed in tumor tissue from B16F10 melanoma xenograft mice (Fig. 10E). In addition, Tip-DC

development induced by Poly6 treatment was inhibited in IFNAR1 KO mice, further supporting *in vitro* findings (Fig. 3F) that Tip-DC development by Poly6 is IFN-I-dependent (Fig. 10F). Poly6 treatment also enhanced expression of DC maturation markers, such as CD40, CD80, CD86, or MHC class II molecules, in tumor and draining lymph node tissues in MC38-bearing mice (Fig. 11A, 11B). In particular, for maturation markers, CD40 expression in DCs was dramatically induced in both cancer tissue and spleen from Poly6 challenged mice. These data suggest that Poly6 treatment enhances production of Tip-DCs and enhances recruitment into the tumor microenvironment, resulting in effective CD8 T cell-mediated tumor rejection likely via the CD40/CD40L axis.

(A)

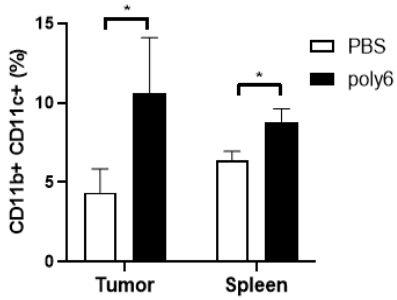
CD11b+ CD11c+ (%)
15
10
5
0
*
*
PBS
poly6
Tumor
Spleen

(B)

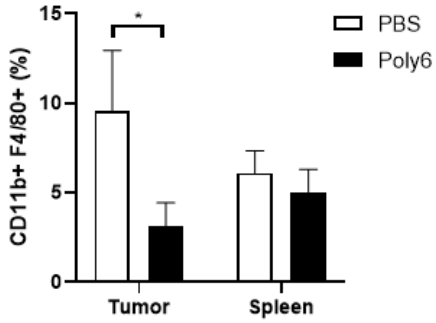
CD11b+ F4/80+ (%)
15
10
5
0
*
PBS
Poly6
Tumor
Spleen

(C)

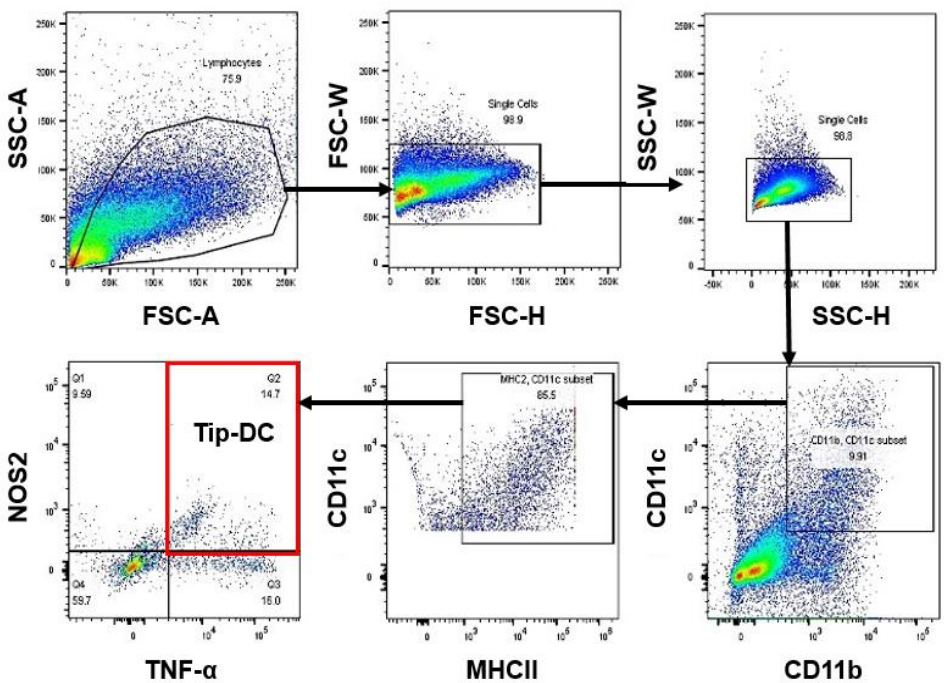
SSC-A
FSC-A
Lymphocytes
75.9
FSC-W
FSC-H
Single Cells
98.9
SSC-W
SSC-H
Single Cells
98.8
NOS2
TNF-α
Tip-DC
Q1
9.59
Q2
14.7
Q4
59.7
Q3
16.0
CD11c
MHCII
MHC2, CD11c subset
85.5
CD11c
CD11b
CD11b, CD11c subset
9.91

(D)

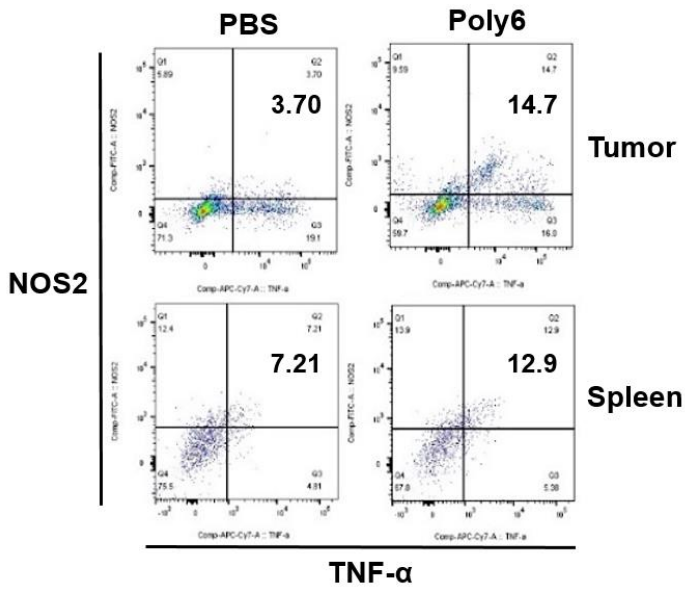
PBS
Poly6
3.70
14.7
Tumor
NOS2
7.21
12.9
Spleen
TNF-α

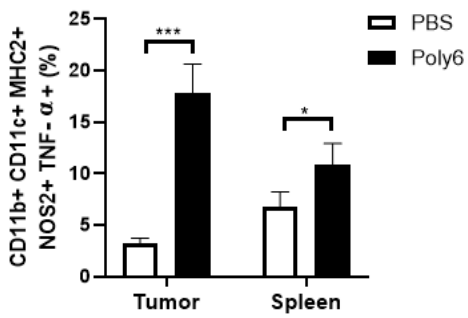
CD11b+ CD11c+ MHC2+
NOS2+ TNF- α + (%)
PBS
Poly6
***
*
Tumor
Spleen

(E)

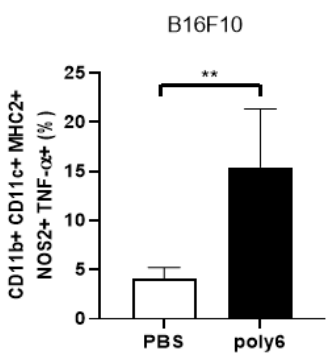
B16F10
CD11b+ CD11c+ MHC2+
NOS2+ TNF-α+ (%)
**
PBS
poly6

(F)

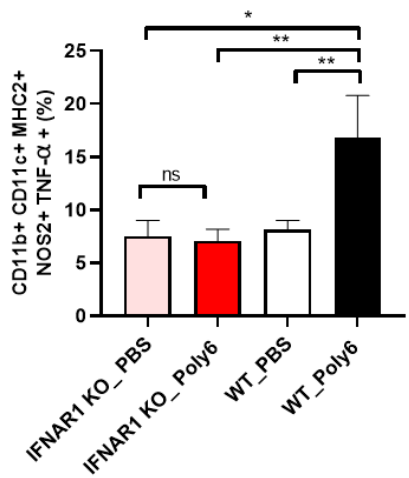
CD11b+ CD11c+ MHC2+
NOS2+ TNF-α + (%)
*
**
**
ns
IFNAR1 KO_ PBS
IFNAR1 KO_ Poly6
WT_PBS
WT_Poly6

Figure 10. Poly6 induces generation of TNF/iNOS-producing DCs (Tip-DCs). (A) The population of CD11b+ CD11c+ dendritic cells in tumor tissue and spleen from MC38-bearing mice were analyzed by FACS. **(B)** The population of CD11b+ F4/80+ macrophages were analyzed by FACS. **(C)** The gating strategy of Tip-DCs was used in tumor tissue, spleen and lymph nodes. This gating was from MC38 tumor tissue on day 16. **(D)** Both intracellular cytokines (TNF-α+, NOS2+) and surface markers (CD11b+, CD11c+, MHC2+) were stained, and this population was termed Tip-DCs. The population of Tip-DCs in tumor tissues and splenocytes from MC38-bearing mice was analyzed by FACS. **(E)** The Tip-DC population in B16F10 melanoma tumor tissues was analyzed by FACS. **(F)** Tip-DC population in MC38 tumor tissues extracted on day 19 from two mouse models, WT and IFNAR1 KO. Significance differences ($^{*}p < 0.05$; $^{**}p < 0.01$; $^{***}p < 0.001$ and $^{****}p < 0.0001$) among different groups are related figures, and the data are presented as the mean ± standard error of mean (SEM) of the mice. Student's t-test was used.

(A)

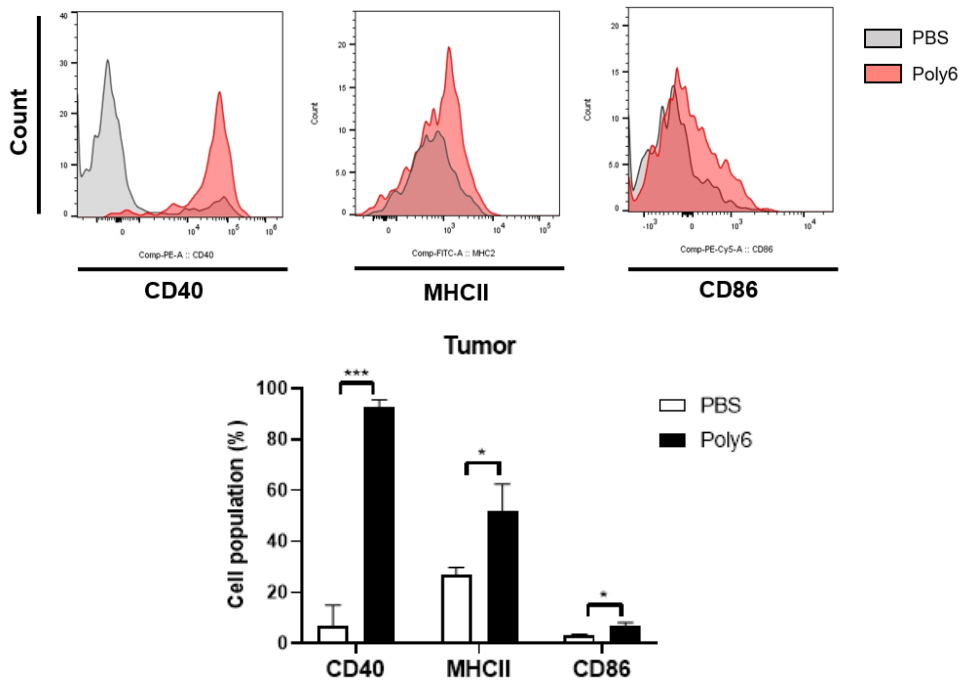
Count
PBS
Poly6
Comp-PE-A :: CD40
Comp-FITC-A :: MHC2
Comp-PE-Cy5-A :: CD86
CD40
MHCII
CD86
Tumor
Cell population (%)
***
*
*
CD40
MHCII
CD86

(B)

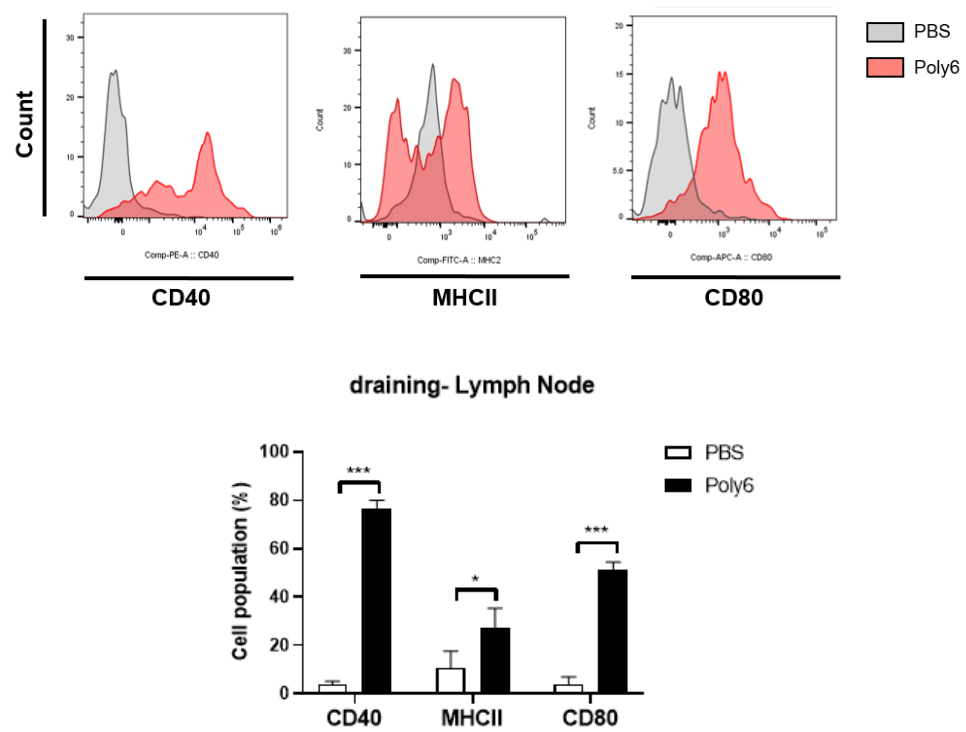
Count
PBS
Poly6
Comp-PE-A :: CD40
Comp-FITC-A :: MHC2
Comp-APC-A :: CD80
CD40
MHCII
CD80
draining- Lymph Node
Cell population (%)
***
*
***
CD40
MHCII
CD80

Figure 11. Poly6 induces an CD40 activation of dendritic cells in vivo.

(A) In tumor tissue, maturation markers for dendritic cells were analyzed. CD40, MHC2 and CD86 markers on DCs in tumor tissue were assessed by FACS analysis (B) In draining lymph nodes, CD40, MHC2 and CD80 maturation markers for dendritic cells were analyzed. Significance differences ($^{*}p < 0.05$; $^{**}p < 0.01$; $^{***}p < 0.001$ and $^{****}p < 0.0001$) among different groups are related figures, and the data are presented as the mean ± standard error of mean (SEM) of the mice. Student's t-test was used.

5. Poly6 leads to direct oncolytic activity of Tip-DCs in a NO-dependent manner.

Previously, it has been reported that innate APCs exert anticancer effects via an iNOS-mediated NO-dependent mechanism [[20], [28], [29]]. Furthermore, Poly6 treatment also attenuated cancer growth and weight, even in nude mice challenged with HBV W4P large surface protein-expressing NIH-3T3 cells (Fig. 12A, 12B). suggesting that innate immune cells could inhibit tumor progression independently of T cells. Therefore, direct oncolytic activity in various cancer cell lines of Tip-DCs developed by Poly6 treatment was evaluated. To this end, Tip-DC-mediated oncolytic activity was evaluated using a coculture system between Poly6-stimulated DC2.4 cells and CFSE-labeled MC38 cells. Poly6 treatment led to increased death of cancer cells in a dose-dependent manner. Furthermore, the oncolytic potential of Poly6 treatment was evaluated in various cancer cell lines using the co-culture system. The Poly6 treated DCs also mediated enhanced oncolytic activity in B16F10 mouse melanoma cancer cells. E0771 mouse breast cancer cells, PanO2 mouse pancreatic cancer cells and MDA231 human breast cancer cells (Fig. 12C).

(A)

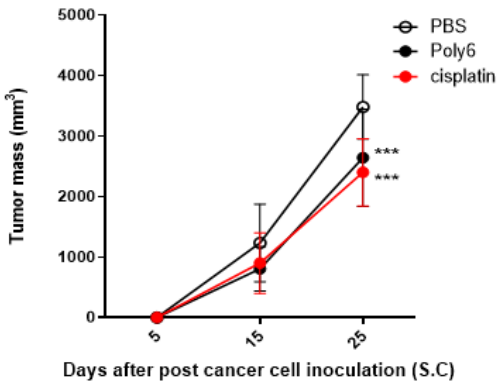
PBS
Poly6
cisplatin
Tumor mass (mm3)
5000
4000
3000
2000
1000
0
5
15
25
***
***
Days after post cancer cell inoculation (S.C)

(B)

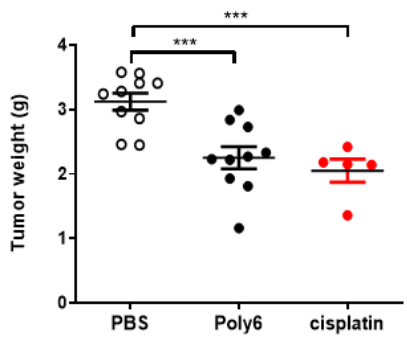
***
***
Tumor weight (g)
4
3
2
1
0
PBS
Poly6
cisplatin

(C)

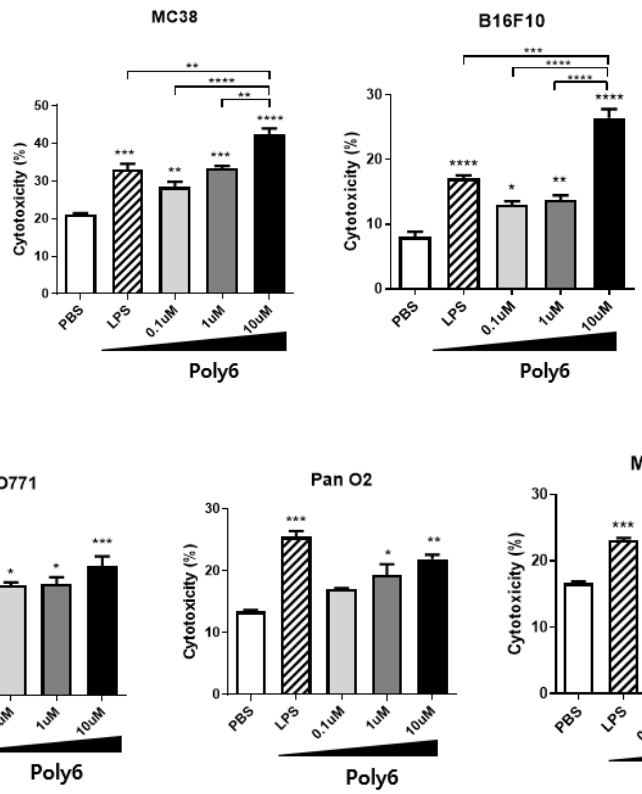
MC38
B16F10
EO771
Pan O2
MDA231
Cytotoxicity (%)
PBS
LPS
0.1uM
1uM
10uM
Poly6

Figure 12. Poly6 leads to the direct oncolytic activity of Tip-DCs.

(A and B) Observation of tumor growth and weight in W4P-LHB cells (1× 108) bearing BALB/c nu/nu mice (n=5~10). (C) Cancer cells (MC38, B16F10, PanO2, EO771, MDA231) were analyzed using a coculture system with Tip-DCs that were generated by Poly6. DC2.4 cells were treated with Poly6 for 48 hr, and CFSE-labeled cancer cells were cocultured with poly6 stimulated DC2.4 cells for 4 hr. 7AAD+ CFSE-labeled dead cancer cells were analyzed by FACS analysis. Significance differences ($^{*}p < 0.05$; $^{**}p < 0.01$; $^{***}p < 0.001$ and $^{****}p < 0.0001$) among different groups are related figures, and the data are presented as the mean ± standard error of mean (SEM) of the mice. Student's t-test was used.

Next, exploration was conducted for finding whether Poly6 treated DCs induce direct tumor killing via a NO-dependent mechanism. To this end, investigation was conducted that the inhibitory effect of an iNOS inhibitor, L-NAME, on the oncolytic activity of Poly6. The addition of L-NAME on Poly6 treated DC2.4 cells led to inhibition of oncolytic activity of Poly6 in various cancer cell lines, including MC38, B16F10 and EO771 cancer cells (Fig. 13A), suggesting that Poly6 treated DCs elicit anticancer effects via the iNOS-NO axis. Also, oncolytic effect of Poly6 in a tumor-bearing mouse model was inhibited in L-NAME treated mice (Fig. 13B). The reduction of tumor growth and weight was not found in both L-NAME and Poly6 treated mice (Fig. 13C, 13D, 13E). Moreover, the Tip-DC generation and T cell activation in tumor tissue by Poly6 were inhibited in L-NAME treated mouse model (Fig. 13F, 13G). In addition, Poly6 treatment leads to generation of an NO-derived oxygen radical, peroxynitrite, known to elicit strong anticancer effects via apoptotic cancer cell death [30, 31]. By immunostaining of nitrotyrosine, an indicator of peroxynitrite formation was evaluated. Actually, Poly6 treated DC2.4 supernatant mediated an intracellular peroxynitrite accumulation within MC38 cancer cells, resulting in shrunken nuclei, a feature of apoptotic cell death, even more so than LPS treated DC2.4 cells (Fig. 14A, 14B).

Furthermore, this enhanced peroxynitrite accumulation in tumor tissues of Poly6 treated MC38 -bearing mice (Fig. 14C). Taken together, these data suggest that Tip-DCs induced by Poly6 exert anticancer effects by direct oncolytic activity via iNOS-dependent production of NO or peroxynitrite.

(A)

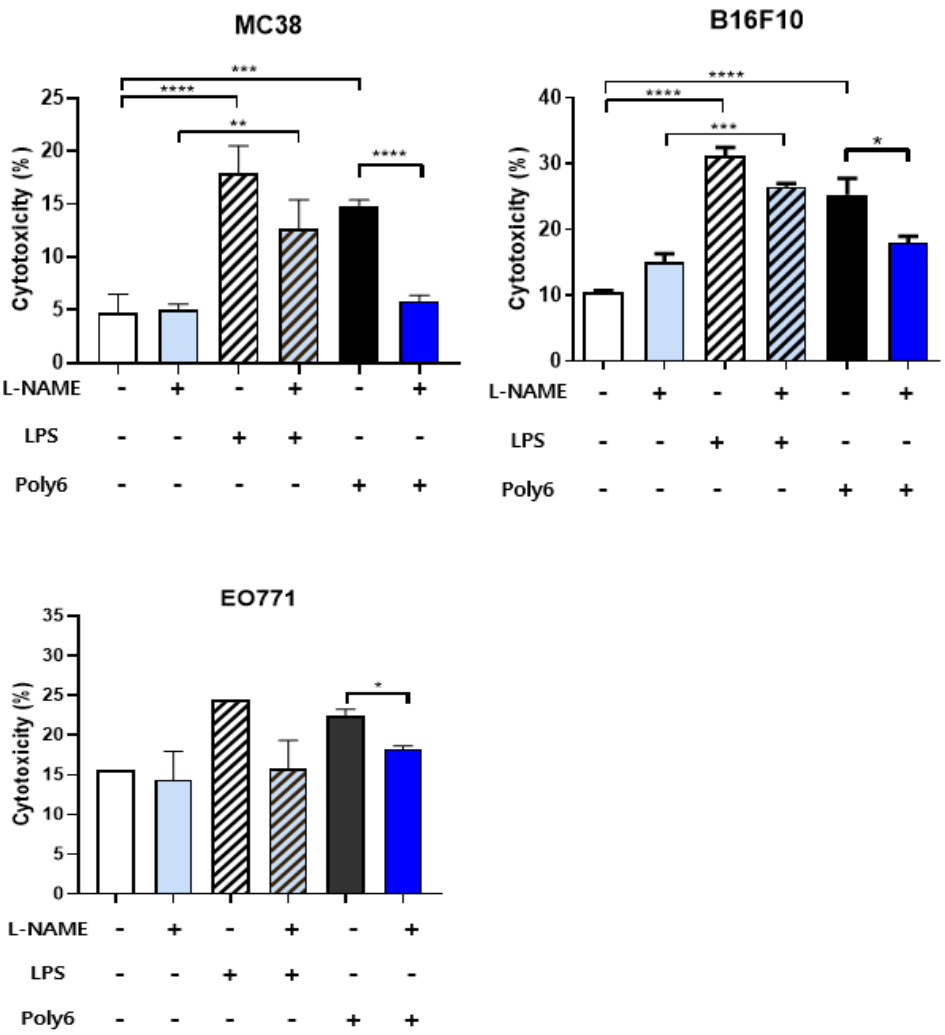
MC38
B16F10
EO771
Cytotoxicity (%)
L-NAME
LPS
Poly6

(B)

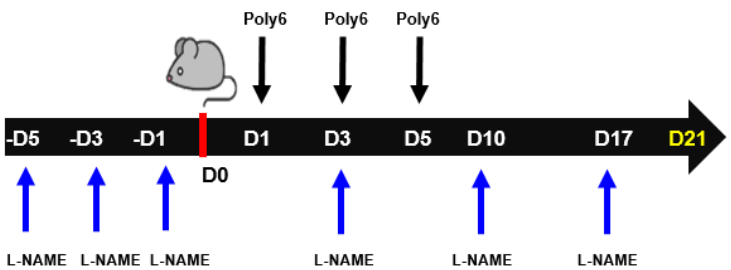
Poly6
Poly6
Poly6
-D5
-D3
-D1
D0
D1
D3
D5
D10
D17
D21
L-NAME
L-NAME
L-NAME
L-NAME
L-NAME
L-NAME

(C)

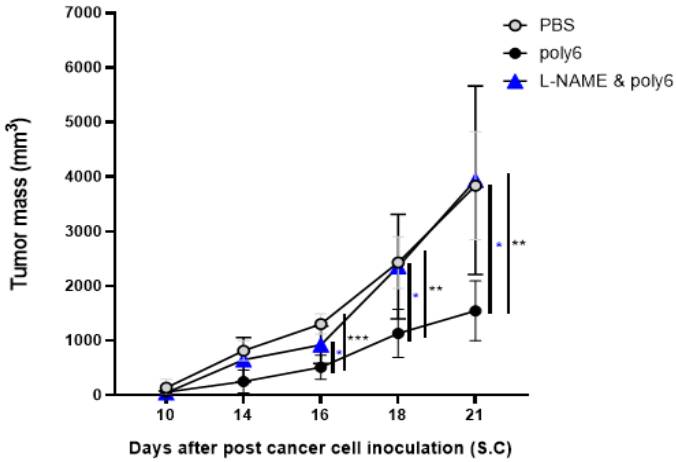
PBS
poly6
L-NAME & poly6
Tumor mass (mm3)
7000
6000
5000
4000
3000
2000
1000
0
10
14
16
18
21
Days after post cancer cell inoculation (S.C)
***
**
*
**
*

(D)

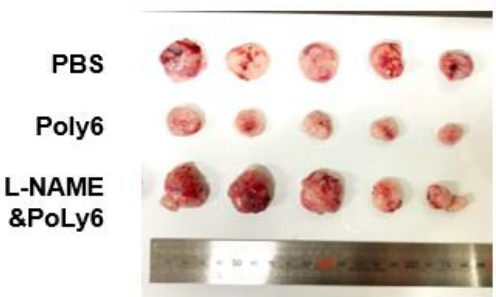
PBS
Poly6
L-NAME
&PoLy6

(E)

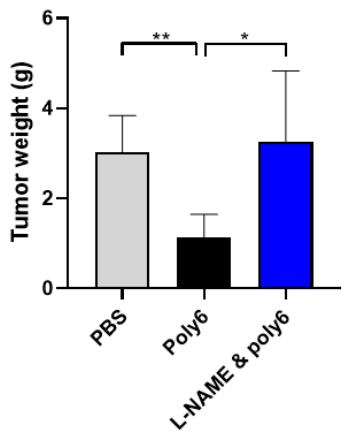
Tumor weight (g)
6
4
2
0
**
*
PBS
Poly6
L-NAME & poly6

(F)

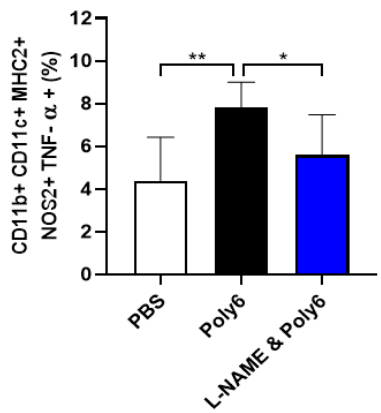
CD11b+ CD11c+ MHC2+
NOS2+ TNF- α + (%)
12
10
8
6
4
2
0
**
*
PBS
Poly6
L-NAME & Poly6

(G)

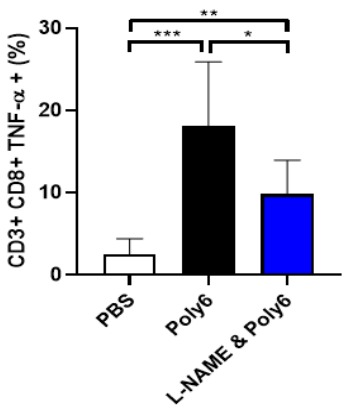
CD3+ CD8+ TNF-α + (%)
30
20
10
0
**
***
*
PBS
Poly6
L-NAME & Poly6

Figure 13. Inhibited anticancer effect of Poly6 in a mouse model by L-NAME treatment.

(A) Inhibited cytotoxicity of cancer cells (MC38, B16F10, EO771) by addition of L-NAME was evaluated by FACS. DC2.4 cells were treated both with Poly6 (10 μM) and/or L-NAME (5mM) for 48 hr. Both Poly6 stimulated DC2.4 cells and CFSE labeled cancer cells were cocultured. 7AAD positive and CFSE labeled cancer cells were evaluated as an oncolytic response. (B) Schematic *in vivo* schedule for NO dependency of anticancer effect of Poly6. Mice were administered L-NAME (2mg/100ul) 3 times via intravenous route before MC38 cancer cell inoculation. After MC38 cells (1×10^6 cells/100 μl) inoculation into C57BL/6 mice, both Poly6 and L-NAME were treated 3 times. (n=5). (C) Comparison of tumor growth followed by treatment with Poly6 or L-NAME. (D) Images of tumors on day 21. (E) Weight of MC38 cancer after sacrifice. (F) Tip-DC population and (G) TNF-α producing T cell population of tumor tissues on day 21 analyzed by flow cytometry. Significance differences ($^{*}p < 0.05$; $^{**}p < 0.01$; $^{***}p < 0.001$ and $^{****}p < 0.0001$) among different groups are related figures, and the data are presented as the mean ± standard error of mean (SEM) of the mice. Student's t-test was used.

(A)

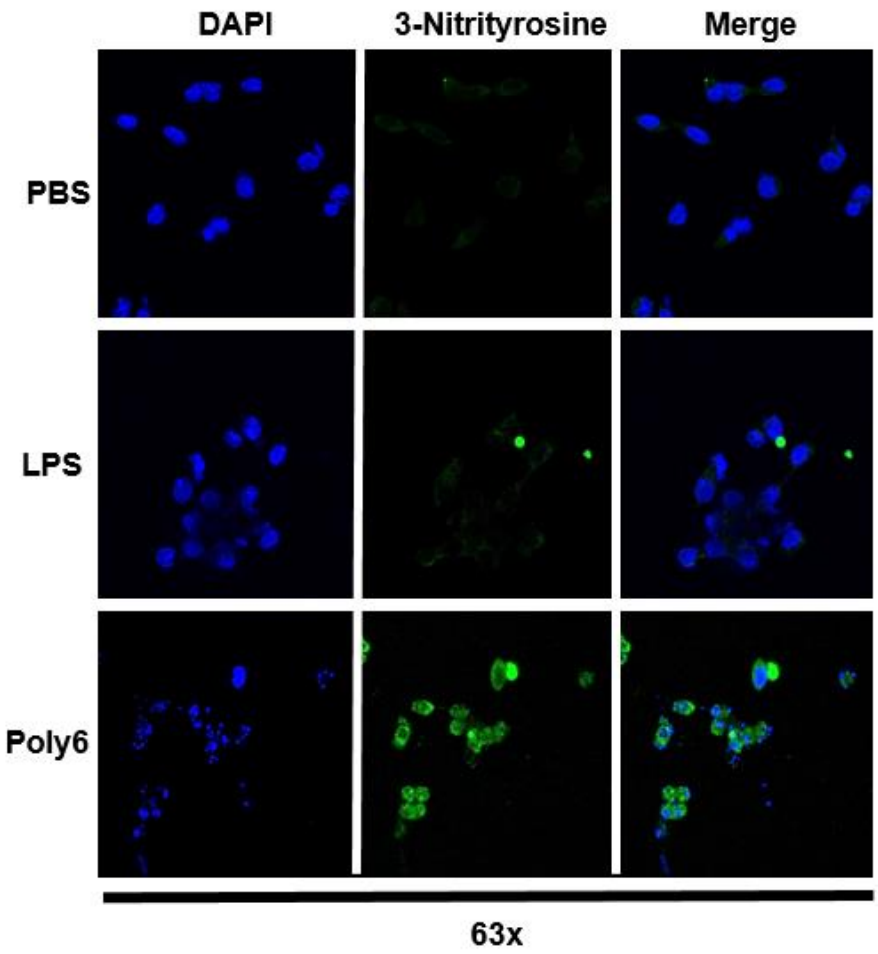
DAPI
3-Nitrityrosine
Merge
PBS
LPS
Poly6
63x

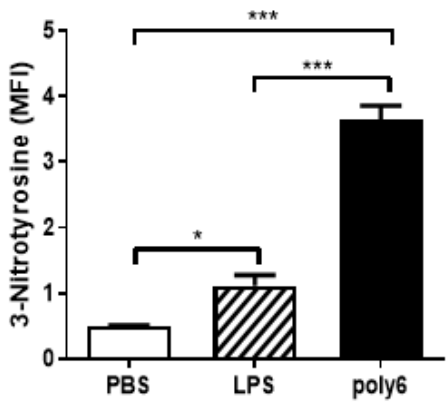
***
***
*
3-Nitrotyrosine (MFI)
0
1
2
3
4
5
PBS
LPS
poly6

(B)

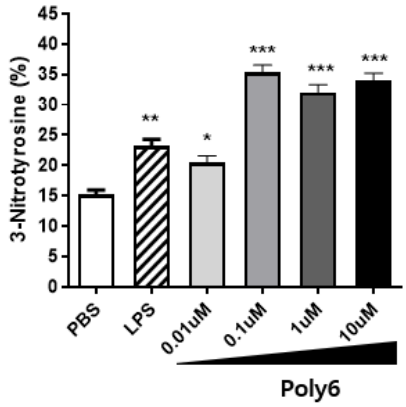
3-Nitrotyrosine (%)
45
40
35
30
25
20
15
10
5
0
**
*
***
***
***
PBS
LPS
0.01uM
0.1uM
1uM
10uM
Poly6

(C)

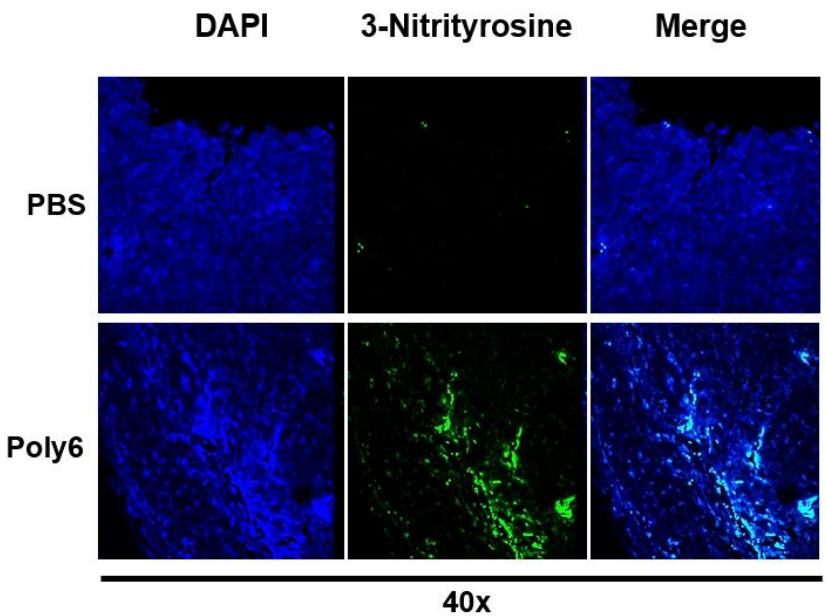
DAPI
3-Nitrityrosine
Merge
PBS
Poly6
40x

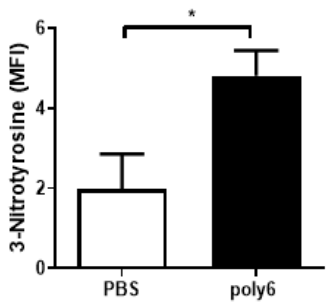
3-Nitrotyrosine (MFI)
6
4
2
0
*
PBS
poly6

Figure 14. Poly6 leads to accumulation of peroxynitrite in cancer cell via NO-dependent manner.

(A) Peroxynitrite levels were evaluated by assessing 3-nitrotyrosine levels. The supernatants of DC2.4 cells treated with Poly6 (1 μM) for 48 hr were treated with MC38 cancer cells for 4 hr. Then, cancer cells were permeabilized and stained with 3-nitrotyrosine antibody. Images were analyzed by confocal microscopy. **(B)** 3-Nitrotyrosine levels were analyzed by FACS. **(C)** Peroxynitrite in tumor paraffin sections was evaluated by 3-nitrotyrosine staining and analyzed by confocal microscopy. These results are representative of two independent experiments. Significance differences ($^{*}p < 0.05$; $^{**}p < 0.01$; $^{***}p < 0.001$ and $^{****}p < 0.0001$) among different groups are shown in related figures, and the data are presented as the mean ± standard error of mean (SEM); $n=3$ biologically independent samples. Student's t-test, one- and two-way ANOVA were used.

6. Combination of Poly6 with anti-PD-L1 Ab treatment exerts an enhanced anticancer effect in mice.

These data indicated that Poly6 exerts anticancer therapeutic effect via apoptotic cancer cell death by Tip-DC mediated NO dependent direct killing and Tip-DC mediated indirect killings by enhanced CTL response. Combinatorial treatment of agents activating CD40/CD40L axis with immune check point inhibitors agents have been reported to have an enhanced anticancer effect [32]. Therefore, an additive anticancer effect of Poly6 treatment with anti-PD-L1 Ab treatment, an immune check point inhibitor, was evaluated [33], in the MC38 -bearing mouse model (Fig. 15A). Combinatorial treatment with Poly6 and anti-PD-L1 demonstrated a significant reduction in tumor growth from 18 days onward compared to single treatment of Poly6 or anti-PD-L1 alone (Fig. 15B, 15C). In addition, after mice were sacrificed, tumor weight was also found to be significantly reduced in mice subject to combinatorial treatment compared to single treatment groups (Fig. 15D). Moreover, an increased population of activated $CD44^+$ T cells in tumor and TNF-α producing effector $CD4^+$ and $CD8^+$T cells in spleen were discoverd (Fig. 16A, 16B). Also, combinatorial treatment significantly increased FasL mRNA in tumor tissue compared to PBS or single treatment groups (Fig. 16C). Taken

together, these data suggest that Poly6 treatment exerts enhanced anticancer effects with anti-PD-L1 Ab treatment in a cancer implanted mouse model.

(A)

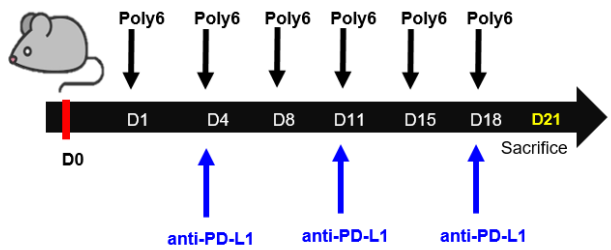
Poly6
Poly6
Poly6
Poly6
Poly6
Poly6
D1
D4
D8
D11
D15
D18
D21
Sacrifice
D0
anti-PD-L1
anti-PD-L1
anti-PD-L1

(B)

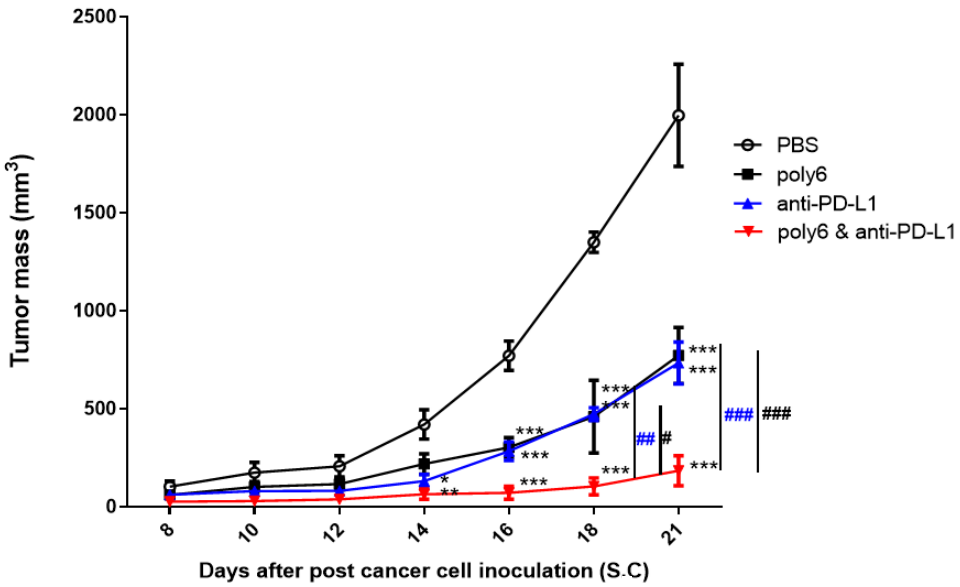
Tumor mass (mm3)
2500
2000
1500
1000
500
0
8
10
12
14
16
18
21
Days after post cancer cell inoculation (S.C)
PBS
poly6
anti-PD-L1
poly6 & anti-PD-L1
***
**
*
##
#
###

(C)

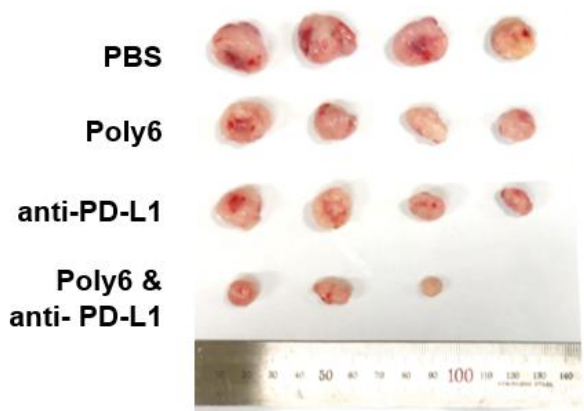
PBS
Poly6
anti-PD-L1
Poly6 &
anti- PD-L1

(D)

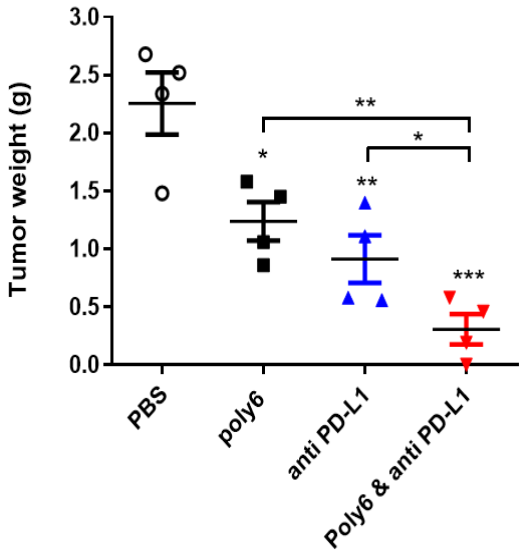

Figure 15. Combination of Poly6 with anti-PD-L1 Ab treatment exerts an enhanced anticancer effect in a tumor-bearing mouse model.

(A) Schematic combination therapy *in vivo* experiment schedule. The Poly6 peptide (10 μg) was subcutaneously injected, and anti-PD-L1 antibody (100 μg) was intraperitoneally injected following the injection schedule. MC38 cancer cells (1×10^6 cells/100 μl) were inoculated on day 0 in C57BL/6 mice. (n=4) (B) Tumor growth was observed for 21 days. (C) Tumor tissue image on day 21. (D) The weight of tumor tissue was compared. Tumor mass was calculated using the following formula: width*width*length*0.52. These results are representative of two independent experiments. Significance differences ($^{*}p < 0.05$; $^{**}p <$

0.01; *** $p < 0.001$ and **** $p < 0.0001$) among different groups are shown in related figures, and the other significance differences # $p < 0.05$; ## $p < 0.01$ and ### $p < 0.001$) are used to compare with the Poly6 and anti-PD-L1 combination group. The data are presented as the mean ± standard error of mean (SEM) of mice. Student's t-test, one- and two-way ANOVA were used.

(A)

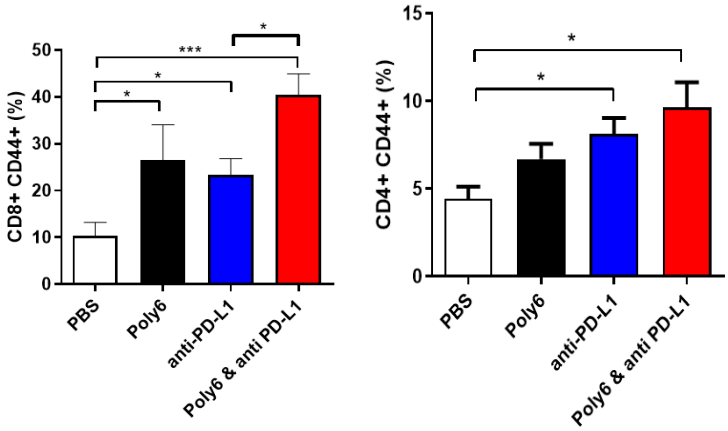
CD8+ CD44+ (%)
50
40
30
20
10
0
*
***
*
*
PBS
Poly6
anti-PD-L1
Poly6 & anti PD-L1
CD4+ CD44+ (%)
15
10
5
0
*
*
PBS
Poly6
anti-PD-L1
Poly6 & anti PD-L1

(B)

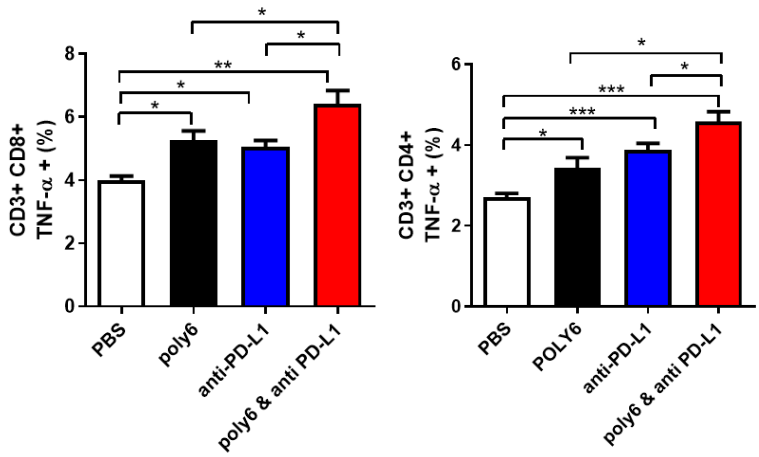
CD3+ CD8+ TNF-α + (%)
8
6
4
2
0
*
**
*
*
PBS
poly6
anti-PD-L1
poly6 & anti PD-L1
CD3+ CD4+ TNF-α + (%)
6
4
2
0
*
*
***
***
*
PBS
POLY6
anti-PD-L1
poly6 & anti PD-L1

(C)

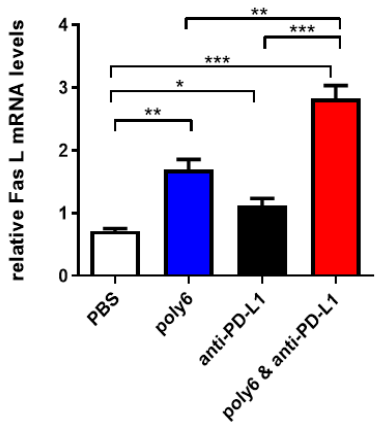
relative Fas L mRNA levels
4
3
2
1
0
**
***
***
*
**
PBS
poly6
anti-PD-L1
poly6 & anti-PD-L1

Figure 16. Combination of Poly6 with anti-PD-L1 Ab treatment exerts an enhanced anticancer effect by inducing activation of CD8+ T cell.

(A) In MC38 tumor tissue on day 21, activated CD44 positive CD4+, CD8+ T cell population was evaluated by FACS analysis. **(B)** The populations of TNF-α or IFN-γ producing CD4+ and CD8+ T cells in the MC38 tumor extracted on day 21 were analyzed by FACS. **(C)** Relative Fas Ligand mRNA levels in MC38 tumor tissue were quantified by qRT-PCR analysis. Significance differences ($^{*}p < 0.05$; $^{**}p < 0.01$; $^{***}p < 0.001$ and $^{****}p < 0.0001$) among different groups are shown in related figures, and the data are presented as the mean ± standard error of mean (SEM) of mice. Student's t-test, one- and two-way ANOVA were used.

DISCUSSION

A DC subset termed Tip-DCs have been reported to play a pivotal role in control or immune pathogenesis in several types of infectious diseases, including *Trypanosoma brucei brucei* [35] and *Listeria monocytogenes* infections [36]. In addition, the novel therapeutic potential of Tip-DCs in the cancer field has recently been introduced [17]. They contribute to cancer inhibition primarily via the CD8 T cell-mediated CTL response by activation of CD40/CD40L in an NO-dependent manner, suggesting that introduction of a new agent favoring Tip-DC development may a feasible option for cancer immunotherapy.

In this study, the potential of Poly6, an HBV-derived 6-mer peptide [18], was examined as a new immune modulating anticancer drug inhibiting tumor progression via enhanced production of Tip-DCs. First, it was found that Poly6 treatment, which can exert anti-HIV-1 effects, induces IFN-I production in DC2.4 cell line and BMDCs via mitochondrial stress mediated cytosolic exposure of mtDNAs (Figs. 2, 3B). Increasing evidence has reported that various drugs targeting molecules modulating host acetylation status, such as histone acetylation transferases (HATs) or histone deacetylases (HDACs), affect mitochondrial homeostasis or

metabolisms [25, 37, 38] or enhance IFN-I productions via acetylation modification of p-STAT-1 [39] or IRF-3 [40]. However, links between cellular modulation and induced IFN-I production found in Poly6 treated DCs need further elucidation in future studies. Enhanced IFN-I production in DCs has been reported as a signature of Tip-DCs [16], which can lead to enhanced TNF and iNOS-mediated NO production or DC maturation, resulting in harnessing T cell-mediated immune responses [14]. Actually, *in vitro* experiments demonstrated that Poly6 treatment leads to increased population of Tip-DCs and maturation of DC cells in an IFN-I-dependent manner (Fig. 3F), resulting in direct oncolytic activity in various cancer cell lines via iNOS-mediated NO and peroxynitrite production (Figs. 12C, 13A, 14). Furthermore, Poly6 vaccination via subcutaneous injection into cancer bearing mice enhanced Tip-DC production and their recruitment into the tumor microenvironment (Fig. 10), resulting in direct cancer cell killing via NO or peroxynitrite production and inhibition of tumor progression indirectly via the CD8 T cell-mediated CTL response (Figs. 9, 10). It has also been reported that enhanced CD8 T cell-mediated CTL response induced by Tip-DCs is primarily due to augmentation of the CD40-CD40L pathway [14]. Consistently, *in vivo* data showed that Poly6 vaccination also led to strong

enhancement of CD40 expression in tumor infiltrated DCs (Fig. 11), compared to other DC costimulatory molecules, CD80, CD86 or MHC class II.

Generally, CD40-CD40L interaction between CD4+ T cells and dendritic cells (DCs) primes DCs to activate CD8+ T cell-mediated CTL- response [41-43]. Therefore, CD40-CD40L also represents an attractive target pathway for cancer immunotherapy. Many cancer immunotherapies using CD40 agonists to therapeutically activate DCs and other myeloid cells have been developed to date [44, 45]. Since single-agent immunotherapy is generally ineffective for the majority of patients with advanced cancers [46], the combined approach of multiple therapeutic agents is implemented to achieve complete remission and cures for cancer patients. Particularly, CD40 agonists enhance anticancer immune responses synergistically with several types of immune check point inhibitors [33]. Consistent with this notion, our data demonstrate that Poly6, a new CD40 inducer, also leads to an enhanced cancer inhibition with anti PD-L1 Ab (Figs. 15, 16).

Of note, it has also been reported that increased CD40 expression can lead to enhanced IFN-I production via the STING-dependent axis [47]. Therefore, despite still being not proven, it is likely that the enhanced IFN-I production observed in Poly6

treated DCs may be due to enhanced CD40 expression. However, relationships between CD40, IFN-I and Poly6 treatment in Tip-DC development need to be elucidated in the future.

Poly6 could induce anticancer effects via direct action in cancer cells in vivo. However, in this study, Poly6 was challenged into mice via an SC route, not via IV route, in a separate region from the site of cancer cell inoculation, suggesting that anticancer effects of Poly6 observed in this study were achieved only via DC-mediated immune response. Hence, Poly6 injection via SC route seems to minimize the risk of side effect by the injection route. Furthermore, Poly6 is capable of inducing DC activation and maturation, providing a rationale regarding its use as an adjuvant for several vaccine modules, including protein-based subunit vaccine or DNA vaccine, as well as cancer immunotherapy. This possibility will be addressed in the future.

In conclusion, these data revealed that Poly6 treatment elicits a strong antitumor immune response in mice, possibly via IFN-I dependent Tip-DC inducing capacity, contributing to tumor clearance by two arms, one for direct cancer cell killing by Tip-DCs in an iNOS-dependent NO and peroxynitrite production manner and the other for indirect killing by CD8+ T cell-mediated CTL-response via a CD40-CD40L pathway dependent mechanism,

suggesting the potential use of Poly6 as an adjunctive immunotherapy capable of enhancing the effect of immune check points (Fig. 17).

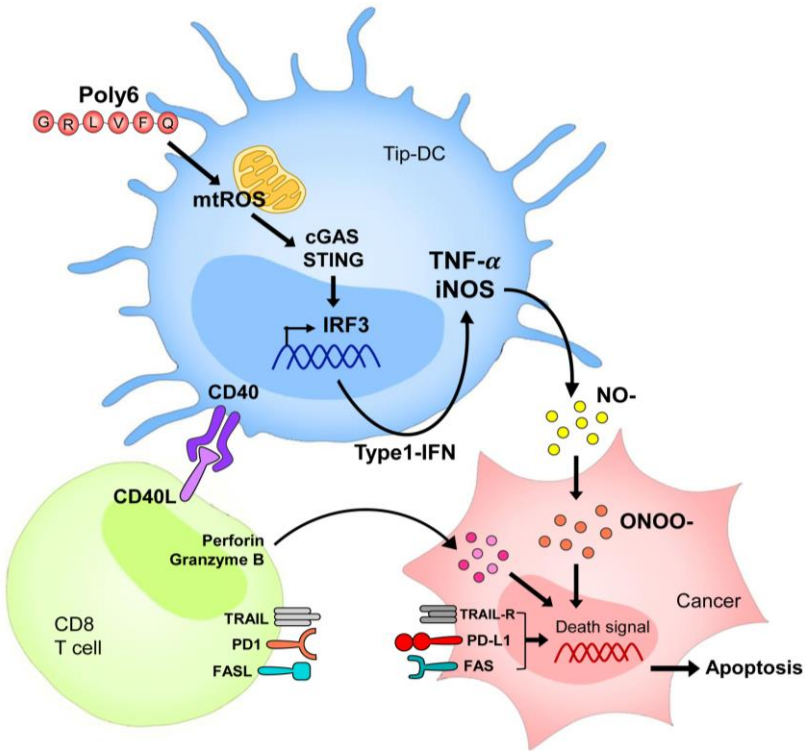

Figure 17. Schematic graphical presentation indicating the anticancer effects of Poly6 via Tip-DCs and activated CD8+ T cells.

Poly6 strongly induces DC maturation and leads to development of Tip-DC in a mitochondrial stress mediated IFN-I dependent manner. In tumor microenvironment, Tip-DCs can induce anticancer responses with two arms. In one hand, Tip-DCs exert iNOS - NO mediated direct oncolytic activity via generation of NO derived oxygen radical, peroxynitrite. In the other hand, CD8+ T cells activated by Tip-DCs via CD40-CD40L axis can induce tumor progress suppression via CTL responses.

REFERENCE

[1] S.J. Oiseth, M.S. Aziz, Cancer immunotherapy: a brief review of the history, possibilities, and challenges ahead, J Cancer Metastasis Treat, 3 (2017) 250-261.

[2] M. Schuster, A. Nechansky, R. Kircheis, Cancer immunotherapy, Biotechnology Journal: Healthcare Nutrition Technology, 1 (2006) 138-147.

[3] S.A. Rosenberg, Overcoming obstacles to the effective immunotherapy of human cancer, Proceedings of the National Academy of Sciences, 105 (2008) 12643-12644.

[4] E. Tcyganov, J. Mastio, E. Chen, D.I. Gabrilovich, Plasticity of myeloid-derived suppressor cells in cancer, Current opinion in immunology, 51 (2018) 76-82.

[5] I. Marigo, L. Dolcetti, P. Serafini, P. Zanovello, V. Bronte, Tumor-induced tolerance and immune suppression by myeloid derived suppressor cells, Immunological reviews, 222 (2008) 162-179.

[6] D.I. Gabrilovich, S. Ostrand-Rosenberg, V. Bronte, Coordinated regulation of myeloid cells by tumours, Nature Reviews Immunology, 12 (2012) 253-268.

[7] Y. Liu, X. Cao, Intratumoral dendritic cells in the anti-tumor

immune response, Cellular & molecular immunology, 12 (2015) 387-390.

[8] S. Amigorena, A. Savina, Intracellular mechanisms of antigen cross presentation in dendritic cells, Current opinion in immunology, 22 (2010) 109-117.

[9] A. Ballestrero, D. Boy, E. Moran, G. Cirmena, P. Brossart, A. Nencioni, Immunotherapy with dendritic cells for cancer, Advanced drug delivery reviews, 60 (2008) 173-183.

[10] M. Datta, L.M. Coussens, H. Nishikawa, F.S. Hodi, R.K. Jain, Reprogramming the tumor microenvironment to improve immunotherapy: emerging strategies and combination therapies, American Society of Clinical Oncology Educational Book, 39 (2019) 165-174.

[11] C. Shi, T. Liu, Z. Guo, R. Zhuang, X. Zhang, X. Chen, Reprogramming tumor-associated macrophages by nanoparticle-based reactive oxygen species photogeneration, Nano letters, 18 (2018) 7330-7342.

[12] A. Sica, C. Porta, S. Morlacchi, S. Banfi, L. Strauss, M. Rimoldi, M.G. Totaro, E. Riboldi, Origin and functions of tumor-associated myeloid cells (TAMCs), Cancer Microenvironment, 5 (2012) 133-149.

[13] K. Bian, F. Ghassemi, A. Sotolongo, A. Siu, L. Shauger, A. Kots,

F. Murad, NOS-2 signaling and cancer therapy, IUBMB life, 64 (2012) 676-683.

[14] I. Marigo, S. Zilio, G. Desantis, B. Mlecnik, A.H. Agnellini, S. Ugel, M.S. Sasso, J.E. Qualls, F. Kratochvill, P. Zanovello, T cell cancer therapy requires CD40-CD40L activation of tumor necrosis factor and inducible nitric-oxide-synthase-producing dendritic cells, Cancer Cell, 30 (2016) 377-390.

[15] H. Kim, S.-Y. Lee, Y.-M. Choi, B.-J. Kim, HBV polymerase-derived peptide exerts an anti-HIV-1 effect by inhibiting the acetylation of viral integrase, Biochemical and biophysical research communications, 501 (2018) 541-546.

[16] P. Dresing, S. Borkens, M. Kocur, S. Kropp, S. Scheu, A fluorescence reporter model defines "Tip-DCs" as the cellular source of interferon β in murine listeriosis, PloS one, 5 (2010) e15567.

[17] S. Ali, R. Mann-Nüttel, A. Schulze, L. Richter, J. Alferink, S. Scheu, Sources of type I interferons in infectious immunity: plasmacytoid dendritic cells not always in the driver's Seat, Frontiers in Immunology, 10 (2019) 778.

[18] S.-A. Lee, H. Kim, Y.-S. Won, S.-H. Seok, Y. Na, H.-B. Shin, K.-S. Inn, B.-J. Kim, Male-specific hepatitis B virus large surface protein variant W4P potentiates tumorigenicity and induces gender

disparity, Molecular cancer, 14 (2015) 23.

[19] S.-Y. Lee, S.-B. Yang, Y.-M. Choi, S.-J. Oh, B.-J. Kim, Y.-H. Kook, B.-J. Kim, Heat-killed Mycobacterium paragordonae therapy exerts an anti-cancer immune response via enhanced immune cell mediated oncolytic activity in xenograft mice model, Cancer Letters, 472 (2020) 142-150.

[20] T.-C. Wu, K. Xu, R. Banchereau, F. Marches, I.Y. Chun, J. Martinek, E. Anguiano, A. Pedroza-Gonzalez, G.J. Snipes, J. O'Shaughnessy, Reprogramming tumor-infiltrating dendritic cells for CD103+ CD8+ mucosal T-cell differentiation and breast cancer rejection, Cancer immunology research, 2 (2014) 487-500.

[21] M. Fauskanger, O.A.W. Haabeth, F.M. Skjeldal, B. Bogen, A.A. Tveita, Tumor killing by CD4+ T cells is mediated via induction of inducible nitric oxide synthase-dependent macrophage cytotoxicity, Frontiers in immunology, 9 (2018) 1684.

[22] Y.-M. Choi, H. Kim, S.-A. Lee, S.-Y. Lee, B.-J. Kim, A telomerase-derived peptide exerts an anti-hepatitis B virus effect via mitochondrial DNA stress-dependent Type I interferon production, Frontiers in Immunology, 11 (2020).

[23] D. Zhang, R. Shi, W. Xiang, X. Kang, B. Tang, C. Li, L. Gao, X. Zhang, L. Zhang, R. Dai, The Agpat4/LPA axis in colorectal cancer cells regulates antitumor responses via p38/p65 signaling in

macrophages, Signal transduction and targeted therapy, 5 (2020) 1-13.

[24] J. Auwerx, T.Y. Li, A conserved role of CBP/p300 in mitochondrial stress response and longevity, The FASEB Journal, 34 (2020) 1-1.

[25] M.A. Zaini, C. Müller, T.V. de Jong, T. Ackermann, G. Hartleben, G. Kortman, K.-H. Gührs, F. Fusetti, O.H. Krämer, V. Guryev, A p300 and SIRT1 regulated acetylation switch of C/EBPα controls mitochondrial function, Cell reports, 22 (2018) 497-511.

[26] A.P. West, W. Khoury-Hanold, M. Staron, M.C. Tal, C.M. Pineda, S.M. Lang, M. Bestwick, B.A. Duguay, N. Raimundo, D.A. MacDuff, Mitochondrial DNA stress primes the antiviral innate immune response, Nature, 520 (2015) 553-557.

[27] B.-R. Kim, B.-J. Kim, Y.-H. Kook, B.-J. Kim, Mycobacterium abscessus infection leads to enhanced production of type 1 interferon and NLRP3 inflammasome activation in murine macrophages via mitochondrial oxidative stress, PLoS pathogens, 16 (2020) e1008294.

[28] X. Duan, C. Chan, W. Lin, Nanoparticle-mediated immunogenic cell death enables and potentiates cancer immunotherapy, Angewandte Chemie International Edition, 58 (2019) 670-680.

[29] F. Vannini, K. Kashfi, N. Nath, The dual role of iNOS in cancer,

Redox biology, 6 (2015) 334-343.

[30] P.M. Thwe, E. Amiel, The role of nitric oxide in metabolic regulation of dendritic cell immune function, Cancer letters, 412 (2018) 236-242.

[31] J. Fraszczak, M. Trad, N. Janikashvili, D. Cathelin, D. Lakomy, V. Granci, A. Morizot, S. Audia, O. Micheau, L. Lagrost, Peroxynitrite-dependent killing of cancer cells and presentation of released tumor antigens by activated dendritic cells, The journal of immunology, 184 (2010) 1876-1884.

[32] C. Szabó, H. Ischiropoulos, R. Radi, Peroxynitrite: biochemistry, pathophysiology and development of therapeutics, Nature reviews Drug discovery, 6 (2007) 662-680.

[33] M. Singh, C. Vianden, M.J. Cantwell, Z. Dai, Z. Xiao, M. Sharma, H. Khong, A.R. Jaiswal, F. Faak, Y. Hailemichael, Intratumoral CD40 activation and checkpoint blockade induces T cell-mediated eradication of melanoma in the brain, Nature communications, 8 (2017) 1-10.

[34] A. Akinleye, Z. Rasool, Immune checkpoint inhibitors of PD-L1 as cancer therapeutics, Journal of hematology & oncology, 12 (2019) 92.

[35] M. Guilliams, K. Movahedi, T. Bosschaerts, T. VandenDriessche, M.K. Chuah, M. Hérin, A. Acosta-Sanchez, L. Ma,

M. Moser, J.A. Van Ginderachter, IL-10 dampens TNF/inducible nitric oxide synthase-producing dendritic cell-mediated pathogenicity during parasitic infection, The Journal of Immunology, 182 (2009) 1107-1118.

[36] N.V. Serbina, T.P. Salazar-Mather, C.A. Biron, W.A. Kuziel, E.G. Pamer, TNF/iNOS-producing dendritic cells mediate innate immune defense against bacterial infection, Immunity, 19 (2003) 59-70.

[37] A. Galmozzi, N. Mitro, A. Ferrari, E. Gers, F. Gilardi, C. Godio, G. Cermenati, A. Gualerzi, E. Donetti, D. Rotili, Inhibition of class I histone deacetylases unveils a mitochondrial signature and enhances oxidative metabolism in skeletal muscle and adipose tissue, diabetes, 62 (2013) 732-742.

[38] M. Fu, W. Shi, Z. Li, H. Liu, Activation of mPTP-dependent mitochondrial apoptosis pathway by a novel pan HDAC inhibitor resminostat in hepatocellular carcinoma cells, Biochemical and biophysical research communications, 477 (2016) 527-533.

[39] J. Liu, L. Jin, X. Chen, Y. Yuan, Y. Zuo, Y. Miao, Q. Feng, H. Zhang, F. Huang, T. Guo, USP12 translocation maintains interferon antiviral efficacy by inhibiting CBP acetyltransferase activity, PLoS Pathogens, 16 (2020) e1008215.

[40] G.T. Melroe, L. Silva, P.A. Schaffer, D.M. Knipe, Recruitment

of activated IRF-3 and CBP/p300 to herpes simplex virus ICP0 nuclear foci: potential role in blocking IFN-β induction, Virology, 360 (2007) 305-321.

[41] S.P. Schoenberger, R.E. Toes, E.I. Van Der Voort, R. Offringa, C.J. Melief, T-cell help for cytotoxic T lymphocytes is mediated by CD40–CD40L interactions, Nature, 393 (1998) 480-483.

[42] S.R.M. Clarke, The critical role of CD40/CD40L in the CD4-dependent generation of CD8+ T cell immunity, Journal of leukocyte biology, 67 (2000) 607-614.

[43] M.F. Bachmann, L. Hunziker, R.M. Zinkernagel, T. Storni, M. Kopf, Maintenance of memory CTL responses by T helper cells and CD40-CD40 ligand: antibodies provide the key, European journal of immunology, 34 (2004) 317-326.

[44] G.L. Beatty, Y. Li, K.B. Long, Cancer immunotherapy: activating innate and adaptive immunity through CD40 agonists, Expert review of anticancer therapy, 17 (2017) 175-186.

[45] R.H. Vonderheide, M.J. Glennie, Agonistic CD40 antibodies and cancer therapy, AACR, 2013.

[46] K. Foley, V. Kim, E. Jaffee, L. Zheng, Current progress in immunotherapy for pancreatic cancer, Cancer letters, 381 (2016) 244-251.

[47] X. Yao, J. Wu, M. Lin, W. Sun, X. He, C. Gowda, S. Bolland, C.A.

Long, R. Wang, X.-z. Su, Increased CD40 expression enhances early STING-mediated type I interferon response and host survival in a rodent malaria model, PLoS pathogens, 12 (2016) e1005930.

국문 초록

B형 간염 바이러스 중합효소 유래 펩타이드의 TNF 및 iNOS 발현 수지상세포 활성화를 통한 항암 효과에 관한 연구

양 수 빈

서울대학교 대학원
의과학과 의과학전공
지도교수 김 범 준

최근, B형 간염 바이러스에서 유래한 Poly6 펩타이드가 인간 면역결핍 바이러스에 대한 항바이러스 효과에 기여하는 것이 밝혀진 바 있다. 본 연구에서는 Poly6를 수지상 세포와 종양 이식 마우스 모델에 투여함으로써, Poly6의 항암 면역 치료 잠재력을 확인하고자 하였다.

생체 외 실험의 연구 결과로써, Poly6가 미토콘드리아 스트레스를 유도하여 제 1형 인터페론 (IFN-I) 의존적으로 TNF 및 iNOS-생산 수지상세포 (Tip-DC) 형성을 유도한다는 것을 확인하였다. 또한 생체 내 실험으로써, 마우스 유래 대장 선암종인 MC38 세포가 이식 된 마우스에 Poly6의 투여는 질소 산화물 (NO) 의존적으로 직접 세포 사멸을 유도하고, CD40 활성화를 통한 Tip-DC 매개 CD8 세포 독성 T 림프구 (CTL) 활성화에 따른 간접적 사멸을 유도하여 종양 형성을

약화시켰다. 이에 더하여, 종양 이식 마우스 모델에서, 면역 체크 포인트 억제제 중 하나인 항-PD-L1 항체와 Poly6를 함께 처리하였을 때 항암 효과를 향상시키는 것을 확인하였다.

결론적으로, 이와 같은 결과들은, Poly6가 Tip-DC 활성화를 통해 단독으로 항암 효과를 보임으로써, 항암 펩타이드로서의 가능성을 보여주었다. 그리고, Poly6와 항-PD-L1의 혼합을 통한 향상된 항암 효과를 확인하였기에, 항암 면역 치료보조제로서 Poly6의 가능성을 보여주었다.

주요어 : B형 간염 바이러스 유래 Poly6 펩타이드, 종양괴사인자 그리고 산화질소 합성효소 생산 수지상세포, 제 1형 인터페론, CD40, 종양 면역 치료

학번 : 2018-23838